

A multi-stage optimization framework for battery electric bus deployment and renewable energy hubs with stochastic energy management and

Downloaded from: https://research.chalmers.se, 2026-11-05 14:47 UTC

Citation for the original published paper (version of record):

Pan, S., Liu, X., Liu, X. et al (2027). A multi-stage optimization framework for battery electric bus deployment and renewable energy
hubs with stochastic energy management and resilience analysis. Transportation Research, Part C: Emerging Technologies, 194. http://dx.doi.org/10.1016/j.trc.2026.106065

N.B. When citing this work, cite the original published paper.

research.chalmers.se offers the possibility of retrieving research publications produced at Chalmers University of Technology. It covers all kind of research output: articles, dissertations, conference papers, reports etc. since 2004. research.chalmers.se is administrated and maintained by Chalmers Library

(article starts on next page)

Transportation Research Part C 194 (2027) 106065



Contents lists available at ScienceDirect

Transportation Research Part C

journal homepage: www.elsevier.com/locate/trc



A multi-stage optimization framework for battery electric bus deployment and renewable energy hubs with stochastic energy management and resilience analysis

Shouzheng Pan [a], Xiaohan Liu [b], Xiaoyue Cathy Liu [a,*], Xiaolei Ma [c], Ran Wei [d]

[a] Department of Civil & Environmental Engineering, University of Utah, 110 Central Campus Dr. Suite 2000, Salt Lake City, UT, 84112, the United States of America
[b] Department of Architecture and Civil Engineering, Chalmers University of Technology, Göteborg, Sweden
[c] School of Transportation Science and Engineering, Beihang University, Beijing, China
[d] School of Public Policy, University of California at Riverside, Riverside, CA, the United States of America

ARTICLE INFO

Keywords:
Battery electric bus
Renewable energy hub
Mobile charging unit
Stochastic optimization
Operational robustness

ABSTRACT

The global electrification of bus fleets has advanced significantly in recent years, yet critical technological and operational challenges persist. First, many existing methodologies for battery electric bus (BEB) deployment focus on cost minimization, often using just enough charging stations to meet demand. This limited setup creates rigid schedules that are vulnerable to delays or charger failures, leading to charging station congestion and service disruptions. Second, large-scale BEB systems often depend on both in-depot and on-route charging, resulting in high charging costs. To address these challenges, this study proposes a multi-stage optimization framework. Stage 1 ensures a cost-effective and robust deployment plan by considering in-depot charging activities, differentiated charger costs and integrating mobile charging units (MCUs) as backup solutions. Stage 2 transforms charging stations into profitable renewable energy hubs by incorporating solar photovoltaic (PV) systems and battery energy storage to reduce grid dependence and generate revenue through surplus energy sales. Stage 3 develops detailed MCU operational strategies to mitigate the impacts of charger failures and bus line delays. The model is applied to a city-scale public transit network in the State of Utah, United States. Results show that MCUs significantly reduce the operational delays and enhance system resilience, while the integration of PV and storage reduces charging costs and increases profitability, particularly during summer months. A comprehensive sensitivity analysis is conducted to identify the most influential parameters affecting system cost, energy performance, and resilience. This research offers practical guidance for public transit agencies in both BEB deployment and renewable energy investment planning.

1. Introduction

Transportation electrification has become a mainstream global trend driven by environmental concerns over greenhouse gas emission and urban air quality. Among the various efforts, battery electric bus (BEB) deployment is accelerating across many countries.

* Corresponding author.
E-mail address: cathy.liu@utah.edu (X.C. Liu).

https://doi.org/10.1016/j.trc.2026.106065
Received 6 January 2026; Received in revised form 21 August 2026; Accepted 4 October 2026
Available online 7 October 2026
0968-090X/© 2026 The Authors. Published by Elsevier Ltd. This is an open access article under the CC BY license (http://creativecommons.org/licenses/by/4.0/).

For instance, China had deployed over 554,000 BEBs by 2024, accounting for 80 % of its total bus fleet (State Council of China, 2024). Cities like Shenzhen have already achieved full bus fleet electrification (ITDP, 2018). In the United States, several cities and states, such as Chicago, Boston, Denver, and California, have committed to zero-emission transit targets (He et al., 2022). However, the cost of electrification remains a significant barrier. A recent study from Germany shows that full fleet electrification increases overall costs by approximately 12 % (Sistig et al., 2025). Beyond capital investment, many transit agencies face high operational expenses post-electrification, particularly related to electricity costs, which presents a sustained financial burden (Jeffers et al., 2021). Integrating renewable energy sources, such as solar photovoltaic (PV), offers a promising strategy to offset these electricity costs. But the inherent uncertainty of renewable energy, driven by external factors such as weather, poses significant challenges for its reliable use in BEB charging operations (Zhao et al., 2024). All these hinder large-scale BEB deployment and highlight the need for strategies that not only reduce upfront costs but also enhance long-term operational profitability and resilience.

BEB deployment problem is commonly modeled through mathematical optimization that address bus replacement strategies, scheduling, and charging station planning (Dirks et al., 2022; Zhou et al., 2020; He et al., 2023a). Many of these models rely on simplifying some assumptions, particularly in large-scale BEB deployment contexts, which may overlook factors critical to real-world implementation. For example, some models incorporate both in-depot and on-route charging but oversimplify critical cost and operational elements, such as charging station types, charger power levels, and operational robustness (Zhou et al., 2020; He et al. 2023a). A closer look at charging station modeling reveals that while many studies configure on-route charging stations in detail, they often treat in-depot charging with simplified assumptions (Ye et al., 2022). A common approach is to assume that each BEB begins the day at the start terminal with a fully charged battery, without explicitly modeling the location, capacity, or scheduling of in-depot chargers, or the overnight charging process (Li et al., 2024). In practice, however, in-depot overnight charging plays a critical role in system performance (Wang et al., 2025a). Factors such as the distance between depots and start terminals can result in vehicles arriving at the first terminal with less than a full charge, which in turn affects subsequent charging needs and station deployment decisions. BEBs also have varying overnight dwell times at depots, which adds complexity to scheduling and energy management. Yet very few studies have examined the detailed operational and infrastructural implications of depot-based charging within large-scale BEB system. From a renewable energy perspective, depots are particularly important: they typically provide larger, less space-constrained areas for PV installation, enabling greater potential for onsite renewable generation compared to on-route charging stations.

In modeling charger costs, most studies assume uniform installation costs across all chargers (Lim et al., 2023). In practice, though, charger installation expenses vary considerably: the first charger at an on-route charging station typically incurs higher costs than additional chargers installed at the same site. Ignoring this cost heterogeneity may lead to suboptimal deployment strategies, for example, favoring one-charger installations across many stations rather than deploying multiple chargers at fewer, high-demand locations.

Even after deployment, long-term operational cost and pricing complexity remain key challenges. Fast on-route charging can drive up electricity expenses, especially when used during peak hours (Johnson et al., 2020). In-depot charging, on the other hand, are typically performed off-peak, follows different tariff structure. While most existing models adopt simple time-of-use pricing, actual utility tariffs, e.g. those applied by Utah Transit Authority (UTA), combine peak-demand charges with energy-usage tiers (Wang et al., 2025b; RMP, 2024). Similar rate policies are observed in cities such as New York and Denver (CARB, 2022; Atlas Public Policy, 2023). Accurately modeling these rate structures is essential for evaluating the economic feasibility of BEB systems. Beyond minimizing costs, generating operational profit is an increasingly desirable goal. Incorporating renewable energy, particularly PV, into charging infrastructure has been widely studied as a strategy to reduce grid dependence (Liu et al., 2024; Ozturk et al., 2025). However, few studies jointly optimize charging operations and renewable generation to balance PV uncertainty, grid pricing, and potential energy sales.

In addition to cost, resilience is another important consideration in the BEB system. Models that minimize only deployment cost tend to produce narrow and inflexible charging windows, making operations sensitive to arrival delays or charger failures. One study shows that the failure of a single charger can reduce station service capacity by 34% (Foda et al., 2023). This vulnerability is even more pronounced at stations equipped with only one charger, where a single failure can halt all charging activity, disrupt service reliability. An emerging solution is the use of mobile charging units (MCUs) - portable, battery-equipped vehicles capable of delivering off-grid charging at flexible locations. MCUs are already adopted in commercial charging applications to handle uncertain demand (Godfrey and Sipiora, 2023). Yet their potential as emergency backup for public transit has not been fully explored. In addition, BEB system with renewable energy also face resilience challenge. The stochastic nature of solar generation adds energy generation uncertainty, making it necessary to evaluate not only operational resilience but also the robustness of profit (Mouli et al., 2016).

To address these limitations, we propose a multi-stage optimization framework that jointly models BEB deployment and renewable energy hub operation. In Stage 1, the model minimizes deployment cost while enhancing system resilience by incorporating MCUs to offset delays and charger failures. Stage 2 builds on this foundation and upgrade charging stations into renewable energy hubs through the integration of PV systems and energy storage, with the objective of maximizing profit under solar generation uncertainty. In Stage 3, the model minimizes disruption-related operational costs by optimizing MCU dispatch and relocation decisions under charger failures and BEB delays. The key contributions of this study are:

- A multi-stage optimization framework that enables end-to-end planning of BEB deployment, renewable energy hub operations, and MCU operations under uncertainty, capturing the dynamic and interactive decision-making process across infrastructure investment and long-term operations;

- A BEB deployment model that incorporates differentiated charger-cost structures and MCU-based backup strategies to enhance system resilience; and
- A stochastic optimization model for urban-scale renewable energy hubs, capturing the effects of dynamic electricity tariffs, solar generation uncertainty, energy storage constraints, and spatial heterogeneity across charging hubs.

The remainder of this paper is organized as follows. Section 2 reviews literature on deployment optimization, resilience, MCUs, and renewable energy integration in BEB systems. Section 3 describes the proposed multi-stage optimization model in detail. Section 4 introduces the case study area and data. Section 5 presents the results from Stage 1, which addresses BEB deployment; and Stage 2, which integrates solar PV and energy storage into an urban-scale energy hub; and Stage 3, which develops the detailed MCU operational strategies under simulated disruptions. Section 6 discusses additional model improvements and extensions. Finally, Section 7 concludes the study and outlines potential directions for future research.

2. Literature review

BEB deployment modeling often requires the incorporation of specific components to better capture real-world operational conditions. These modeling components can be broadly categorized into two groups: fleet-focused elements and charging station-related elements. Fleet-focused modeling often considers factors such as vehicle types (Tang et al., 2023), battery capacities (Zhang et al., 2022), battery degradation (Wang et al., 2025a), uncertain energy consumption (Zhou et al., 2022), stochastic demand (Wu et al., 2022; Bazarnovi et al., 2025), and stochastic travel times (Tang et al., 2019). Charging station modeling includes aspects such as smart charging power allocation (Ye et al., 2022), tiered charging rates (Bao et al., 2023), waiting times (Bazarnovi et al., 2025), and layout and configurations of in-depot and on-route charging stations (He et al., 2023b).

For charging station components, most existing models place greater emphasis on the spatial layout and scheduling of on-route charging stations. For example, He et al. (2019) explored the use of fast chargers at on-route stations in an eight-line bus network. Results show that effective charger deployment can greatly reduce the BEB battery cost and total deployment cost. An (2020) developed a stochastic integer programming model to optimize on-route charging station locations and roughly estimated the overnight in-depot charging costs. While some studies model in-depot charging exclusively within single-depot environments (Wang et al., 2025a; Davatgari et al., 2024), others employ simplified charging strategies in a BEB system. Tang et al. (2019) incorporated virtual in-depot stations that can estimate BEB fleet size more accurately. A static-dynamic scheduling model was tested on a six-line network, showing its effectiveness in preventing operational disruptions. He et al. (2023a) developed a BEB schedule optimization model but simplified the representation of in-depot overnight charging. The model was applied to a single BEB line using five days of operational data. Results demonstrate that optimized charging strategies can significantly reduce in-depot charging costs. Few other papers consider both on-route and in-depot charging stations, but they often simplify the operational details of both. For example, Zhou et al. (2020) developed a bi-objective optimization model and applied it to a city-level transit system. While the model estimated the required number of on-route and in-depot charging stations, it did not incorporate detailed in-depot charging schedules. Overall, studies focusing on charging stations tend to prioritize on-route charging optimization, particularly in large-scale applications. While some models incorporate in-depot charging, they often oversimplify the scheduling details and cost structures, and are typically limited to small-scale networks involving only a few bus lines. Few studies have comprehensively addressed large-scale BEB deployment that simultaneously integrates high-resolution overnight charging schedules and detailed in-depot station characteristics, such as the number of chargers and operational costs.

With specific components considerations in place, the selection of model objectives is another critical aspect of BEB deployment modeling. As cost reduction is often the top priority for transit agencies, most existing models adopt cost minimization as the primary objective. This typically includes capital expenditures such as BEB procurement and charger installation (both in-depot and on-route), as well as ongoing operational costs (He et al., 2023c; Tang et al., 2019). Additional costs considered include delay costs (Tang et al., 2019), maintenance costs (Can et al., 2025), battery and charging costs (Li et al., 2024), driver costs (He et al., 2023c), passenger delay penalties (Tang et al., 2023), and high-voltage infrastructure costs (Dirks et al., 2022). While existing studies have covered major cost categories, they often overlook critical aspects that can significantly influence both model outcomes and practical implementation. These include variations in charging costs across different station types and installation costs associated with different charger power levels - factors that are especially important in large-scale BEB systems. Beyond cost minimization, alternative modeling objectives include reducing greenhouse gas (GHG) emissions (Ye et al., 2022), charging frequency (Cokyasar et al., 2023), and maximizing service levels (Yi et al., 2023). Several multi-objective approaches also considered cost jointly together with environmental equity (Zhou et al., 2020) or reduction of non-BEB mileage (He et al., 2022).

Besides cost and service-oriented objectives, recent studies have also examined the robustness of BEB operation. Tang et al. (2019) introduced a buffer-distance and rescheduling strategy to improve BEB schedule robustness under traffic uncertainty. Yi et al. (2023) integrated agent-based modeling with a robustness optimization framework to address the charging station location problem, aiming to maximize service coverage under potential disruptions. The results show that the optimized station layout can significantly enhance the overall charging performance of the system. Fan et al. (2025) investigated the impact of weather uncertainty on charging station operations. To balance economic feasibility with environmental sustainability, they developed a globalized robust optimization model. Their results demonstrate that employing a probabilistic risk measure can effectively mitigate the risk of unmet charging demand. Zhang et al. (2025) proposed a robustness assessment framework for BEB networks based on complex network theory. Their results demonstrate that the failure of a single charging station can trigger cascading impacts across the network. However, most robustness-oriented models neglect deployment cost considerations, while cost-minimization models often treat robustness only through post hoc

sensitivity analysis. Chen et al. (2023), for instance, developed a network flow model to evaluate the cost-efficient resource allocation and performed a sensitivity analysis to assess system robustness. Their results indicated that increasing charging capacity beyond a certain threshold can enhance robustness but yields diminishing economic returns. Overall, only a few studies have integrated both deployment cost and robustness into a unified optimization framework.

To enhance the operational robustness and flexibility of BEB, the use of MCUs has emerged as a promising solution. Existing literature predominantly highlights three key benefits of MCUs: complementing fixed infrastructure, improving spatial coverage, and serving as flexible components within integrated energy systems. First, MCUs are widely explored as a flexible supplement to fixed charging infrastructure, especially for managing peak demand or addressing unexpected charging needs. Afshar et al. (2022), for instance, developed an optimization framework to identify optimal MCU deployment strategies, highlighting their effectiveness as a flexible supplement to fixed charging during peak demand periods. This strategic value is further supported by studies that emphasize the economic and operational benefits of deploying MCUs over fixed stations under specific conditions. Zhang et al. (2020) found that MCUs can significantly reduce user waiting times and are more cost-effective, particularly under conditions of low station utilization and high land costs. Second, MCUs are shown to significantly improve spatial coverage and service quality, particularly in dense urban or underserved areas. Chen et al. (2024) assessed the feasibility of MCU deployment using agent-based simulation, demonstrating that MCUs can improve spatial coverage and enhance users' charging experiences cost-effectively. Third, and more recently, MCUs have been explored as components of integrated energy systems within broader energy architectures, demonstrating their sophisticated role beyond simple backup charging. Duan et al. (2025) developed a multi-event scenario-based model to schedule MCU charging from solar PV and discharging to EV customers. The results indicate that this integrated strategy can substantially reduce operating costs and enhance renewable energy utilization. Collectively, these studies suggest that MCUs are ideal candidates for flexible and backup charging in electrified transportation. Yet, few have investigated their role in BEB systems for enhancing system robustness against disruptions and failures, which is the focus of this paper.

The integration of renewable energy, particularly solar PV, into BEB charging systems is a critical strategy for reducing grid dependence. Research in this area shows a dual focus: operational optimization and economic viability. On the operational front, studies incorporate PV, energy storage, and advanced scheduling (Liu et al., 2023) to align intermittent renewable energy generation with dynamic BEB charging demands. For example, Najafi et al. (2025) considered solar PV integration in the power distribution network with BEB charging. Their results showed that renewable energy integration can reduce violations of technical constraints in the power distribution network. However, the specific impacts of depot-level solar PV deployment were not explicitly considered. Ren et al. (2022) proposed a control strategy to align PV generation with BEB charging demand, demonstrating improved system utilization and reduced grid reliance. Economically, literature confirms that renewable energy integration significantly reduces operational costs and carbon emissions (Islam et al., 2022). Furthermore, research explores the potential of converting charging stations into energy

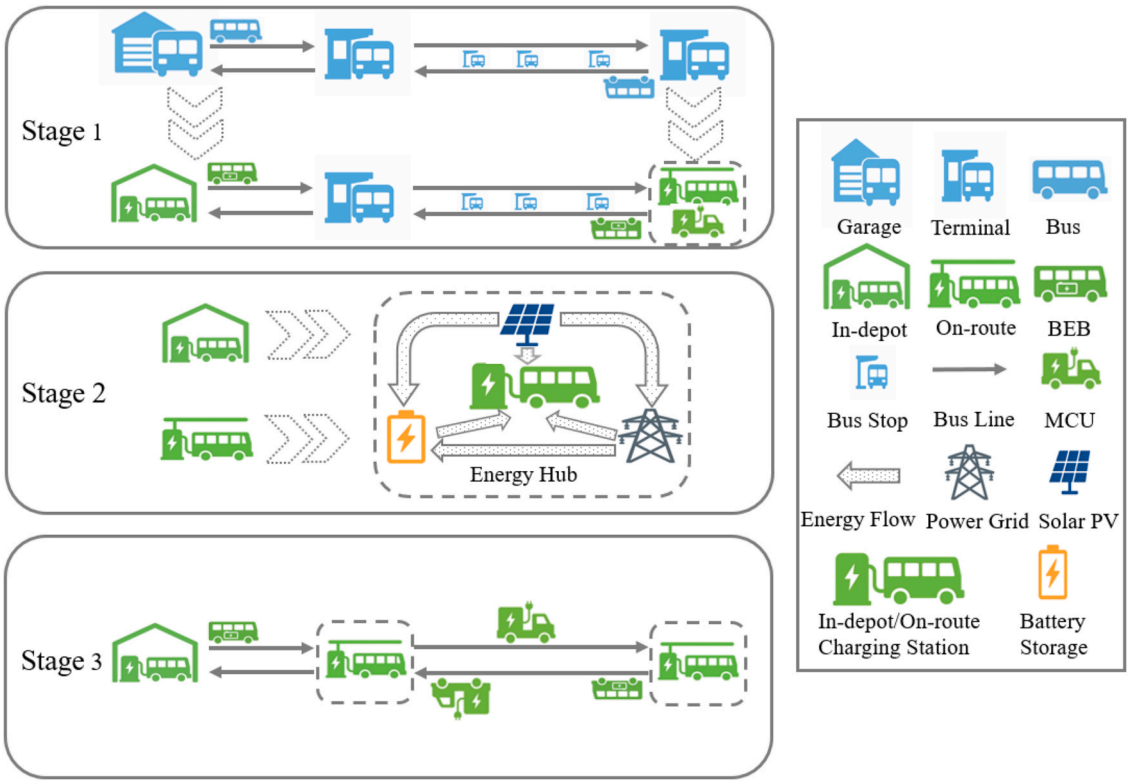


Fig. 1. Overview of BEB system deployment and the transition to renewable energy hubs.

hubs that can generate revenue from surplus energy sales (Liu et al., 2024). However, studies caution that profitability is highly sensitive to external and internal factors like weather uncertainty, PV deployment constraints and energy storage sizing. Despite these advancements in short-term charging and economic analysis, the system-level robustness and long-term scalability of renewable-integrated BEB operations against uncertainties remain largely unexplored.

3. Problem Description and Formulation

This study investigates a practical planning problem in which public transit agencies aim to transition from a conventional bus system to a BEB system by setting an anticipative bus replacement target. To ensure long-term operational sustainability, agencies might also seek to integrate renewable energy infrastructure in potential charging stations, such as solar PV systems. To address this challenge, we propose a comprehensive and transferable multi-stage optimization framework, as illustrated in Fig. 1. A conventional bus system consists of buses, routes, intermediate stops, terminal stations, and garages. As shown in Stage 1 of Fig. 1, each bus route is served by a fleet of buses that begin service from an assigned depot, travel to the origin terminal, and operate along a predefined

Table 1
Summary of Stage 1 notations.

Sets	Description
$\mathscr{A}$	Set of feasible MCU relocation arcs $(j,j') \in \mathscr{A}$
$\mathscr{B}_j$	Set of bus-sequence pairs that may charge at station j
$\mathscr{G}$	Set of candidate in-depot charging stations, $g \in \mathscr{G}$
$\mathscr{I}$	Set of buses in the fleet, $i \in \mathscr{I}$
$\mathscr{I}_g$	Set of buses located at depot g, $i \in \mathscr{I}_g$
$\mathscr{J}$	Set of candidate on-route charging stations,$j \in \mathscr{J}$
$\mathscr{K}_i$	Ordered set of route segments (sequences) for bus i,$k \in \mathscr{K}_i$
$\mathscr{M}$	Set of MCUs,$m \in \mathscr{M}$
$\mathscr{T}$	Set of time steps in a day, $t \in \mathscr{T}$
$\mathscr{T}_j$	Set of time steps with overlapping bus presence at station j
$\mathscr{V}_{j,t}$	Set of buses dwelling at station j at time step t
Parameters	
c^{bat}	Battery cost per kWh ($/kWh)
c^B	Capital cost of replacing a bus with a BEB
c^G	Capital cost of building one in-depot charger
c^F, c^S	Capital cost of first and subsequent on-route chargers
c^m	Capital cost of MCUs
D	Operating days per year
$d_{i,k}$	Distance covered in route segment k of bus i
d_i^{ff}	First and final segment distance from depot to first stop of bus i
E^{Full}, E^{Max}, E^{Min}	Full, max, and min energy capacity of BEB battery (kWh)
κ^G	Overnight charging capacity per depot charger
κ^O	Capacity (simultaneous sessions) per on-route charger
L_i	Number of route segments for bus i
M	A large number used for big-M constraints and binary logic constraints
N^{cycle}	Battery cycle life
P	Charger power (kW)
Y	Planning horizon (years)
y_j^C	Available charger deployment area of station j (m^2)
α	Small positive constant for enforcing logic
$\delta_{i,k}$	1 if charging of bus i at step k is peak
Δ^C	Unit area of one charger (m^2)
η	Energy efficiency (kWh/mile)
ϕ	Charging power penalty factor
$\tau_{i,k}$	Time available for charging at step k of bus i (minutes)
ω^{deg}	Weight factor for degradation cost
$\aleph$	Bus replacement target
Decision variables	
R	Number of mobile charging units
$X_{i,k}$	1 if bus i is charged at segment k
Y_g^G	Number of chargers to install at depot g
Y_j^S	Number of subsequent chargers to install at station j
Z_i	1 if bus i is replaced with BEB
Γ_j	1 if first charger is built at station j
Auxiliary variables	
$e_{i,k}$	Energy level of bus i at step k
$M_{j,t}$	Number of chargers used at station j and time t
$q_{i,k}$	Depth of discharge of bus i at segment k (kWh)
$\theta_{j,t^{hour}}$	Whether need mobile charging station at station j and time t^{hour}

sequence of stops until reaching the destination terminal. A single bus may complete multiple trips on different routes within a service day. Upon completing its scheduled runs, each bus returns to the depot for overnight storage and maintenance. In BEB system, depots can be retrofitted as in-depot charging facilities, selected terminals are upgraded with on-route chargers, and traditional buses are replaced with BEBs with limited driving ranges.

Stage 1 addresses the infrastructure deployment and fleet transition problem. It determines which buses are to be replaced, where to locate charging stations (both in-depot and on-route), how many chargers to install, charging schedule, and how to allocate MCUs as backup resources. Stage 2 focuses on renewable energy integration problem, where each charging facility is modeled as a local energy hub. It optimizes the installation of solar PV panels and battery energy storage at depots and terminals, and determines real-time power exchanges among PV systems, power grid, energy storage, and BEBs. For example, as shown in Stage 2 of Fig. 1, PV-generated energy can be used to charge BEBs, stored for later use, or be exported to the grid for profit. Stage 3 addresses operational resilience under disruption scenarios. It optimizes the real-time dispatch and relocation of MCUs to mitigate charging shortages caused by charger failures or bus operation delays. The model determines MCU movements, charging support assignments, and energy usage over time to minimize unmet charging demand and maintain charging service continuity across the network. Together, these three stages form a resilient, end-to-end planning framework that captures both infrastructure deployment and long-term energy management performance under operational and renewable uncertainties. The detailed formulation of each stage is presented in the following subsections.

3.1. Stage 1

The notation used in the Stage 1 model is summarized in Table 1.

Objective

The objective function of Stage 1 is to minimize the total cost of transitioning the fleet to BEBs:

$$min \sum_{g\in\mathscr{G}} c^G Y_g^G + \sum_{j\in\mathscr{J}} \left(c^F \Gamma_j + c^S Y_j^S\right) + \sum_{i\in\mathscr{I}} c^B Z_i + c^m R + \omega^{deg} YD \sum_{i\in\mathscr{I}} \sum_{k\in K_i} \frac{c^{bat} \phi q_{i,k}}{N^{cycle} DoD^{use}} \tag{1}$$

Fixed charger deployment cost $\sum_{g\in\mathscr{G}} c^G Y_g^G + \sum_{j\in\mathscr{J}} \left(c^F \Gamma_j + c^S Y_j^S\right)$ includes the cost of in-depot charger, first on-route charger which is more expensive and subsequent on-route chargers. $\sum_{i\in\mathscr{I}} c^B Z_i$ is the BEB purchase cost. $c^m R$ is the MCU deployment cost. Considering the long-term operation of BEB systems, unhealthy charging schedules, such as frequent charging/discharging cycles, high charging power, and deep battery discharge, may accelerate battery degradation and increase lifecycle costs. Therefore, the last term in the objective function incorporates a lifecycle-equivalent battery degradation cost (Liu et al., 2021; Wang et al., 2020).

$$\sum_{i\in\mathscr{I}} Z_i \geq \aleph \tag{2}$$

$$X_{i,k} \leq \Gamma_j \quad \forall j \in \mathscr{J}, \forall (i,k) \in \mathscr{B}_j \tag{3}$$

$$X_{i,k} \leq Z_i \quad \forall i \in \mathscr{I}, k \in \mathscr{K}_i \tag{4}$$

$$\sum_{(i,k)\in\mathscr{T}_{j,t}} X_{i,k} = M_{j,t} \quad \forall j \in \mathscr{J}, t \in \mathscr{T}_j \tag{5}$$

$$Y_j^s \leq M\Gamma_j \quad \forall i \in \mathscr{I} \tag{6}$$

$$\sum_{i\in\mathscr{I}_g} Z_i \leq \kappa^G Y_g^G \quad \forall g \in \mathscr{G} \tag{7}$$

$$\left(\Gamma_j + \kappa^O Y_j^S\right) \Delta^C \leq y_j^C \quad \forall j \in \mathscr{J} \tag{8}$$

$$M_{j,t} \leq \Gamma_j + \kappa^O Y_j^S + \theta_{j,t^{20}} - \alpha\Gamma_j \quad \forall j \in \mathscr{J}, t \in \mathscr{T}_j, t^{20} \in \{0,1,\cdots,72\} \tag{9}$$

$$\theta_{j,t^{20}} \leq \Gamma_j \quad \forall j \in \mathscr{J}, t^{20} \in \{0,1,\cdots,72\} \tag{10}$$

$$\sum_{j\in\mathscr{J}} \theta_{j,t^{20}} \leq R \quad \forall j \in \mathscr{J}, t^{20} \in \{0,1,\cdots,72\} \tag{11}$$

$$e_{i,0} = Z_i \left(E^{Full} - d_i^{ff} \eta\right) \quad \forall i \in \mathscr{I} \tag{12}$$

Table 2
Summary of Stage 2 notations.

Sets	Description
$\mathscr{J}$	Set of built charging stations, $j \in \mathscr{J}$ and $\mathscr{J} = \mathscr{J}^B \cup \mathscr{J}^G$
$\mathscr{J}^B$	Set of built on-route charging stations,$j \in \mathscr{J}^B$
$\mathscr{J}^G$	Set of built in-depot charging stations,$j \in \mathscr{J}^G$
$\mathscr{T}$	Set of time steps in a day, $t \in \mathscr{T}$
Ω	Set of PV generation scenarios,$s \in \Omega$
Parameters	**Stage 2**
c^{es}	Daily amortized cost of storage per kWh capacity, including installation, operation, and maintenance cost
c^{PV}	Daily amortized cost of PV investment per m^2, including installation, operation, and maintenance cost
C_r	Storage C-rate (max charging/discharging rate as a fraction of capacity)
$d^s_{j,t}$	PV output per unit area at station j, time t, scenario s (kWh/m^2)
M	A large number used for big-M constraints and binary logic constraints
$\mathscr{P}_{j,t}$	Total real-time charging power required by BEBs at station j, time t (kW)
$\mathscr{P}_{\max}$	Maximum allowable grid power draw (kW)
$S^{\max}$	Maximum storage capacity (kWh)
y_j^{PV}	Maximum allowable PV deployment area station j (m^2)
η_{es}	Efficiency of energy storage system
$\lambda^f_{j,t}$	Feed-in tariff or grid value of exported PV at station j, time t ($/kWh)
δ_t^{Peak}	1 if time t is peak period (e.g., 7am–11 pm), 0 otherwise
β^{Depot}	Policy parameter at in-depot station: daily share of tier-1 billing energy
ρ	Tier breakpoint (e.g., 1500 kWh)
β	Policy parameter at on-route station: daily share of tier-1 billing energy
Δ_t	Duration of one time step (in hours, e.g., 1 min = 1/60 h)
π_0	Fixed electricity connection charge
π_1	Rate for first 50 kWh/kW block (peak usage)
π_2	Rate for additional peak kWh
π_{off}	Credit for off-peak charging
π_0^{Depot}, π_1^{Depot}, π_2^{Depot}	Fixed electricity access fee, rate for first 1500 kWh, and rate for additional energy
Decision variables	**Stage 2**
$D^s_{j,t}$	Energy discharged from storage to buses at station j, time t, scenario s (kWh)
$E^s_{j,t}$	State of charge of storage at station j, time t, scenario s (kWh)
$G^{es,s}_{j,t}$	Grid energy sent to storage at station j, time t, scenario s (kWh)
$G^s_{j,t}$	Grid charging power for BEB charging at station j, time t, scenario s (kW)
$P^{es,s}_{j,t}$	PV energy sent to storage at station j, time t, scenario s (kWh)
S_j	Installed energy storage capacity station j (kWh)
$U^s_{j,t}$	PV energy used directly for bus charging at station j, time t, scenario s (kWh)
y_j	PV deployment area of station j (m^2)
Auxiliary variables	**Stage 2**
A^s_j	Additional peak energy usage at station j (kWh)
B^s_j	First-tier (up to 50 kWh/kW) energy block for billing 1 at station j (kWh)
C^s_j	Total daily electricity cost from grid purchases at station j under scenario s ($)
H^s_j	Binary variable: 1 if peak energy exceeds policy threshold, 0 otherwise
$H^{T,s}_j$	Binary variable: 1 if total energy exceeds policy threshold, 0 otherwise
$P^{Peak,s}_j$	Peak grid power draw across the day at station j (kW)
$Q^{T,s}_j, Q^{F,s}_j, Q^{S,s}_j$	Total grid energy, first-block and additional energy charged at in-depot station j (kWh)
$Q^{p,s}_j, Q^{o,s}_j$	Total grid energy during peak and off-peak hours at station j (kWh)
$z^{C,s}_{j,t}$	1 if storage is being charged at station j, time t, 0 otherwise
$z^{D,s}_{j,t}$	1 if storage is discharging at station j, time t, 0 otherwise

$$Z_i E^{Min} \le e_{i,k} \le E^{Full} - X_{i,k}\left(E^{Full} - E^{Max}\right) \quad \forall i \in \mathscr{I}, k \in \{1, \cdots, L_i\} \tag{13}$$

$$e_{i,k} = e_{i,k-1} + X_{i,k} P \tau_{i,k} \Delta_t - Z_i d_{i,k-1} \eta \quad \forall i \in \mathscr{I}, k \in \mathscr{K}_i, k \ge 1 \tag{14}$$

$$e_{i,L_i} = e_{i,L_i-1} - Z_i d_i^{ff} \cdot \eta \quad \forall i \in \mathscr{I} \tag{15}$$

$$e_{i,L_i} \ge Z_i E^{Min} \quad \forall i \in \mathscr{I} \tag{16}$$

$$q_{i,k} \ge e_{i,k-1} - e_{i,k}, \forall i \in I, k \in K_i \tag{17}$$

Constraint (2) enforces the predetermined bus replacement target $\aleph$, making sure the total number of conventional buses converted to BEBs meets (or exceeds) the planning goal. Constraint (3)-(8) define the charging availability & capacity. Constraints (3) and (4) ensure that on-route charging is only permitted at terminal stations with installed chargers and that only BEBs can utilize them. Constraint (5) enforces that the number of BEBs charging at any given time does not exceed the station's charger capacity. The set $\mathscr{V}_{j,t}$ is constructed from historical operational schedules and capture the potential number of buses that may compete for charging service at the same station and time. Constraint (6) links binary and integer variables to guarantee that chargers are installed only at charging stations that are selected for construction. Constraint (7) ensures that a sufficient number of chargers are deployed at in-depot stations to support overnight charging. Constraint (8) limits the number of chargers at each on-route station based on available installation space.

Constraint (9)-(11) determine optimal MCU deployment within the model. Constraint (9) ensures that an MCU is deployed only when all fixed chargers at a charging station are fully occupied. A small positive constant α is introduced to significantly improve computational efficiency, reducing the optimization time from several hours to just minutes. Since prolonged charging peaks require longer MCU occupancy and potentially additional MCU deployment, this constraint is incentivized to reduce peak duration. Together, Constraints (8) and (9) indirectly mitigate excessive charging peaks by limiting charger deployment and discouraging prolonged periods of simultaneous charging. Constraint (10) ensures that MCUs can only be deployed at charging stations where chargers are installed. Constraint (11) calculates the maximum number of MCUs that are being used at any given time for all charging stations. The activation time steps t^{20} are set to 20 minutes to balance the MCU movements and time efficiency.

Constraint (12)-(17) define the energy transition logic. Constraint (12) initializes the battery energy level at the beginning of each operating day. Each BEB departs from the in-depot with a full battery (E^{Full}) and arrives at the first terminal with $E^{\text{Full}} - d_i^{\text{Final}}\eta$ energy remaining, where d_i^{Final} is the distance from depot to the first terminal and η is the energy consumption rate. Constraint (13) ensures that the battery capacity of each BEB remains within 20% to 80% at all stops, terminals, and charging stations in each trip, maintaining operational safety and charging efficiency. For non-electrified buses, energy is allowed to range from 0% to 100%. Constraint (14) models the energy transition across sequential segments of each bus route. Constraints (15) and (16) determine the final energy level as the BEB returns from the last terminal to the in-depot station. Constraint (17) define the depth of each discharge.

3.2. Stage 2

The notation used in the Stage 2 model is summarized in Table 2.

Scenario-based uncertainty representation

To explicitly capture the variability of solar generation, a scenario-based stochastic programming approach is adopted. Let Ω denote the set of PV generation scenarios, where each scenario $s \in \Omega$ represents a typical daily PV generation profile derived from historical data. To capture seasonal and intra-day variability, the historical PV profiles are first divided into four seasons (Winter, Spring, Summer, and Fall). K-means clustering is then applied within each season using features including total daily generation, peak output, and ramping variability. Two representative clusters are generated for each season, representing relatively high-generation and low-generation PV conditions, resulting in a total of eight PV generation scenarios across the year. Each scenario is associated with a probability p_s, determined by the proportion of days represented by the corresponding cluster.

$$p_s = \frac{\text{ClusterSize}_s}{\sum_{s\in\Omega}\text{ClusterSize}_s} \tag{18}$$

where ClusterSize_s denotes the number of historical days assigned to scenario s. These scenarios are used to represent uncertainty on the renewable energy supply side, while on the demand side, a fixed BEB charging demand obtained from Stage 1 is used across all scenarios.

Objective

The objective is to maximize the expected net profit across all energy hubs and scenarios:

$$\max \sum_{s\in\Omega} p_s \sum_{j\in\mathscr{J}} \sum_{t\in\mathscr{T}} \left[\lambda'_{j,t}\left(d^s_{j,t}y_j - U^s_{j,t} - P^{es,s}_{j,t}\right) - C^s_j - c^{PV}y_j - c^{es}S_j\right] \tag{19}$$

where $\lambda'_{j,t}$ represents the electricity value or feed-in tariff, C^s_j is the grid electricity cost under scenario s, and c^{PV} and c^{es} denote the amortized costs of PV and storage investments, respectively.

$$y_j \le y_j^{PV} \quad \forall j \in \mathscr{J} \tag{20}$$

$$P_j^{Peak,\ s} \ge G^s_{j,t} \quad \forall j \in \mathscr{J}^B, \forall t \in \mathscr{T}, s \in \Omega \tag{21}$$

$$G_{j,t}^{s} = \mathscr{P}_{j,t} - \left(U_{j,t}^{s} + \eta_{es} D_{j,t}^{s} - G_{j,t}^{es,s}\right) \Big/ \Delta_t \quad \forall j \in \mathscr{J}, t \in \mathscr{T}, s \in \Omega \tag{22}$$

$$Q_j^{p,s} = \sum_{t \in \mathscr{T}} \delta_t^{Peak} G_{j,t}^{s} \Delta_t \quad \forall j \in \mathscr{J}^B, s \in \Omega \tag{23}$$

$$Q_j^{o,s} = \sum_{t \in \mathscr{T}} \left(1 - \delta_t^{Peak}\right) G_{j,t}^{s} \Delta_t \quad \forall j \in \mathscr{J}^B, s \in \Omega \tag{24}$$

$$\begin{aligned} B_j^s &\le Q_j^{p,s} \\ B_j^s &\le P_j^{Peak,s} \beta \\ B_j^s &\ge Q_j^{p,s} - \left(1 - H_j^s\right) M \\ B_j^s &\ge P_j^{Peak,s} \beta - H_j^s M \end{aligned} \quad \forall j \in \mathscr{J}^B, s \in \Omega \tag{25}$$

$$A_j^s \ge Q_j^{p,s} - P_j^{Peak,s} \beta \quad \forall j \in \mathscr{J}^B, s \in \Omega \tag{26}$$

$$C_j^s = \pi_0 + \pi_1 B_j^s + \pi_2 A_j^s + \pi_{\text{off}} Q_j^{o,s} \quad \forall j \in \mathscr{J}^B, s \in \Omega \tag{27}$$

$$Q_j^{T,s} = \sum_{t \in T} G_{j,t}^{s} \Delta_t \quad \forall j \in \mathscr{J}^{\mathscr{C}}, s \in \Omega \tag{28}$$

$$Q_j^{T,s} = Q_j^{F,s} + Q_j^{S,s} \quad \forall j \in \mathscr{J}^{\mathscr{C}}, s \in \Omega \tag{29}$$

$$\begin{aligned} Q_j^{T,s} &\ge \rho H_j^{T,s} \\ Q_j^{F,s} &\le \rho \\ Q_j^{F,s} &\ge \rho H_j^{T,s} \end{aligned} \quad \forall j \in \mathscr{J}^{\mathscr{C}}, s \in \Omega \tag{30}$$

$$Q_j^{S,s} \le M H_j^{T,s} \quad \forall j \in \mathscr{J}^{\mathscr{C}}, s \in \Omega \tag{31}$$

$$C_j^s = \pi_0^{Depot} + , \pi_1^{Depot} Q_j^{F,s} + , \pi_2^{Depot} Q_j^{S,s} \quad \forall j \in \mathscr{J}^{\mathscr{C}}, s \in \Omega \tag{32}$$

$$E_{j,t}^{s} = E_{j,t-1}^{s} + \eta_{es}\left(P_{j,t}^{es,s} + G_{j,t}^{es,s}\right) - D_{j,t}^{s} \quad \forall j \in \mathscr{J}, t > 0, s \in \Omega \tag{33}$$

$$0.2 S_j \le E_{j,t}^{s} \le S_j \quad \forall j \in \mathscr{J}, t \in \mathscr{T}, s \in \Omega \tag{34}$$

$$E_{j,0}^{s} = S_j, \quad E_{j,T_{\text{end}}}^{s} = S_j \quad \forall j \in \mathscr{J}, s \in \Omega \tag{35}$$

$$P_{j,t}^{es,s} + U_{j,t}^{s} \le d_{j,t}^{s} y_j \quad \forall j \in \mathscr{J}, t \in \mathscr{T}, s \in \Omega \tag{36}$$

$$P_{j,t}^{es,s} + G_{j,t}^{es,s} \le C_r S_j \Delta_t \quad \forall j \in \mathscr{J}, t \in \mathscr{T}, s \in \Omega \tag{37}$$

$$\eta_{es} D_{j,t}^{s} + U_{j,t}^{s} \le \mathscr{P}_{j,t} \Delta_t \quad \forall j \in \mathscr{J}, t \in \mathscr{T}, s \in \Omega \tag{38}$$

$$D_{j,t}^{s} \le C_r S_j \Delta_t \quad \forall j \in \mathscr{J}, t \in \mathscr{T}, s \in \Omega \tag{39}$$

$$P_{j,t}^{es,s} + G_{j,t}^{es,s} \le M z_{j,t}^{C,s} \quad \forall j \in \mathscr{J}, t \in \mathscr{T}, s \in \Omega \tag{40}$$

$$D_{j,t}^{s} \le M z_{j,t}^{D,s} \quad \forall j \in \mathscr{J}, t \in \mathscr{T}, s \in \Omega \tag{41}$$

$$z_{j,t}^{C,s} + z_{j,t}^{D,s} \le 1 \quad \forall j \in \mathscr{J}, t \in \mathscr{T}, s \in \Omega \tag{42}$$

Constraint (20)-(22) define the PV and peak power. Constraint (20) limits the PV deployment area at each energy hub to the available rooftop or ground-mounted space. Constraint (21) defines the peak grid electricity usage within a day, which is used to calculate peak demand charges. Constraint (22) determines the total charging power at each time step, reflecting real-time power flows and accounting for contributions from both PV generation and energy storage.

Constraint (23)-(32) model two billing structures. First one considers peak demand charges with total energy usage which applies to on-route charging hubs. Constraints (23) and (24) divide total electricity usage into peak and off-peak components. Constraint (25) enforces tiered energy pricing rules based on usage thresholds. Constraint (26) identifies the portion of energy that qualifies for the

lower-cost tier, while Constraint (27) calculates the total electricity cost incurred under this pricing scheme. Second one uses different energy usage tiers which applies to in-depot charging hubs. An example about this billing structure with detailed illustration are shown in Tables 11 and 12 of Appendix B. Constraint (28) calculates the total daily energy consumption. Constraint (29) separates the energy use into first-block and additional energy usages for tiered billing. Constraint (30) applies the utility's tiered pricing rules, while Constraint (31) identifies the portion of energy that qualifies for the lower-cost tier. Constraint (32) computes the total electricity cost under this billing scheme.

Constraint (33) models the temporal dynamics of battery energy storage levels across the day. Constraint (34) restricts the state-of-charge (SOC) to remain between 20% and 100% of the total battery capacity. Constraint (35) ensures that the battery begins and ends each day fully charged, maintaining a consistent daily energy cycle. Constraint (36)-(39) limit the PV generation and flow. Constraint (36) ensures that the total PV energy used for BEB charging and energy storage at each time step does not exceed the available PV generation. Constraint (37) limits the charging and discharging power of the energy storage system based on its capacity and C-rate. Constraint (38) guarantees that the combined energy supplied from PV and storage does not exceed BEB charging demand at each station and time step. Constraint (39) restricts the discharge quantity from storage to ensure it remains within feasible operational bounds. Constraints (40) and (41) define the binary control variables that indicate whether the energy storage system is charging or discharging at each time step. Constraint (42) ensures mutual exclusivity, preventing the energy storage system from charging and discharging simultaneously.

3.3. Stage 3

The notation used in the Stage 3 model is summarized in Table 3.

To evaluate the operational resilience of the BEB system and the reliability of MCUs under disruption conditions, a set of operational disruption scenarios is developed first. Based on the baseline charging schedules obtained from Stage 1, disruption scenarios are introduced, including: (1) charger failures at specific stations and time periods; and (2) bus arrival delays propagating through the network. Under each disruption scenario ω, the effective charging capacity is reduced, and the charging demand may exceed available capacity. The resulting unmet charging requirement is defined as:

Table 3
Summary of Stage 3 notations.

Sets	Description
$\mathscr{A}$	Set of feasible MCU relocation arcs $(j,j') \in \mathscr{A}$
$\mathscr{J}$	Set of built charging stations,$j \in \mathscr{J}$
$\mathscr{T}$	Set of time steps in a day, $t \in \mathscr{T}$,$\mathscr{T} = \{0,1,\cdots,H-1\}$
$\mathscr{M}$	Set of MCUs,$m \in \mathscr{M}$
Parameters	
c^e	Electricity price for MCU recharging
c^u	Penalty for unmet residual MCU demand
c^p	Penalty for failing to satisfy the protection requirement
c^r	Fixed cost of one MCU relocation
$\overline{C}$	Maximum MCU charging energy per bin, $P^c\Delta/60$
$\overline{D}$	Maximum MCU discharging energy per bin,$P^d\Delta/60$
$E^{\max}$	MCU battery capacity
H	Total number of time steps in the planning horizon
N^m	Number of available MCUs
$\mathscr{P}$	Set of protected station-time pairs (j,t)
P^c	MCU charging power
P^d	MCU discharging power
$q^{\omega}_{j,t}$	Residual MCU demand at station j, time t, under disruption scenario ω
$U^{\omega}_{j,t}$	Charging demand at station j and time t under disruption scenario ω.
$\overline{Y}^{\omega}_{j,t}$	Available chargers at station j, time t under disruption scenario ω
$\underline{\alpha}$	Minimum SOC ratio
α^0	Initial SOC ratio
Δ	Duration of each time bin, in minutes
$\tau_{j,j'}$	Travel time from station j to j', measured in time bins
$\gamma_{j,j'}$	Energy consumed by an MCU moving from j to j'
Decision variables	
$c_{m,j,t}$	Energy charged into MCU m at station j,t
$p_{j,t}$	Shortage of protection requirement
$u_{j,t}$	Unserved residual MCU demand
$y_{m,j,j',t}$	1 if MCU m departs from station j at time t and moves to station j'
Auxiliary variables	
$a_{m,t}$	1 if MCU m is in charging mode at time t
$d_{m,j,t}$	Energy discharged by MCU m at station j,t
$e_{m,t}$	Battery energy of MCU m at time t
$s_{m,j,t}$	1 if MCU m is located at station j at time t

$$q_{j,t}^{\omega} = \max\left(0, U_{j,t}^{\omega} - \widetilde{Y_{j,t}^{\omega}}\right) \cdot P\Delta_t \tag{43}$$

Objective

Given the disruption-induced demand $q_{j,t}^{\omega}$, we formulate an operational optimization model to determine the deployment and scheduling of MCUs. The objective function minimizes the total operational cost, including unmet charging demand penalty, MCU charging cost, and MCU relocation cost.

$$\min \sum_{j\in\mathscr{J}}\sum_{t\in\mathscr{T}} c^u u_{j,t} + \sum_{m\in\mathscr{M}}\sum_{j\in\mathscr{J}}\sum_{t\in\mathscr{T}} c^e c_{m,j,t} + \sum_{m\in\mathscr{M}}\sum_{(j,j')\in\mathscr{A}}\sum_{t\in\mathscr{T}} c^r y_{m,j,j',t} + \sum_{j\in\mathscr{J}}\sum_{t\in\mathscr{T}} c^p p_{j,t} \tag{44}$$

$$\sum_{j\in\mathscr{J}} s_{m,j,t} \le 1, \qquad \forall m \in \mathscr{M}, t \in \mathscr{T} \tag{45}$$

$$\sum_{j\in\mathscr{J}} s_{m,j,0} = 1, \qquad \forall m \in \mathscr{M} \tag{46}$$

$$\sum_{m\in\mathscr{M}} s_{m,j,t} + p_{j,t} \ge 1, \qquad \forall (j,t) \in \mathscr{P} \tag{47}$$

$$p_{j,t} = 0, \qquad \forall (j,t) \notin \mathscr{P} \tag{48}$$

$$\sum_{(j,j')\in\mathscr{A}} y_{m,j,j',t} \le s_{m,j,t-1}, \qquad \forall m \in \mathscr{M}, j \in \mathscr{J}, t \ge 1 \tag{49}$$

$$s_{m,j,t} = s_{m,j,t-1} - \sum_{(j,j')\in\mathscr{A}} y_{m,j,j',t} + \sum_{\substack{(j',j)\in A \\ t-\tau_{j',j}\ge 0}} y_{m,j',j,t-\tau_{j',j}}, \qquad \forall m \in \mathscr{M}, j \in \mathscr{J}, t \ge 1 \tag{50}$$

$$y_{m,j,j',t} = 0, \qquad \forall m \in \mathscr{M}, (j,j') \in \mathscr{A},\ t + \tau_{j,j'} \ge H \tag{51}$$

$$\sum_{j''\in\mathscr{J}} s_{m,j'',t'} \le 1 - y_{m,j,j',t}, \quad \forall m \in \mathscr{M}, (j,j') \in \mathscr{A}, t < t' < t + \tau_{j,j'} \tag{52}$$

$$c_{m,j,t} \le \overline{C} s_{m,j,t}, \qquad \forall m \in \mathscr{M}, j \in \mathscr{J}, t \in \mathscr{T} \tag{53}$$

$$d_{m,j,t} \le \overline{D} s_{m,j,t}, \qquad \forall m \in \mathscr{M}, j \in \mathscr{J}, t \in \mathscr{T} \tag{54}$$

$$\sum_{m\in\mathscr{M}} d_{m,j,t} + u_{j,t} = q_{j,t}^{\omega}, \qquad \forall j \in \mathscr{J}, t \in \mathscr{T} \tag{55}$$

$$e_{m,0} = E^{\max}\alpha^0, \qquad \forall m \in \mathscr{M} \tag{56}$$

$$e_{m,t} \ge E^{\max}\underline{\alpha} \tag{57}$$

$$e_{m,t+1} = e_{m,t} + \sum_{j\in\mathscr{J}} c_{m,j,t} - \sum_{j\in\mathscr{J}} d_{m,j,t} - \sum_{(j,j')\in\mathscr{A}} \gamma_{j,j'} y_{m,j,j',t}, \qquad \forall m \in \mathscr{M}, t \le H-2 \tag{58}$$

$$\sum_{j\in\mathscr{J}} c_{m,j,t} \le \overline{C} a_{m,t}, \qquad \forall m \in \mathscr{M}, t \in \mathscr{T} \tag{59}$$

$$\sum_{j\in\mathscr{J}} d_{m,j,t} \le \overline{D}\left(1 - a_{m,t}\right), \qquad \forall m \in \mathscr{M}, t \in \mathscr{T} \tag{60}$$

Constraints (45) and (46) ensure that each MCU can be located at only one station at each time interval and is assigned to one initial station at the beginning of the planning horizon. Constraints (47) and (48) define the protection requirements for station–time pairs included in the protection plan generated in Stage 1. Constraints (49) through (52) govern MCU relocation feasibility, travel continuity, and movement timing between charging stations. Constraint (49) ensures that an MCU can depart from a station only if it is physically located at that station in the previous time step. Constraint (50) updates the MCU location status over time by tracking departures from the current station and arrivals from previously initiated relocation trips, while explicitly accounting for travel times between stations. Constraint (51) prevents infeasible relocations that cannot be completed within the remaining planning horizon. Constraint (52) ensures travel continuity by prohibiting an MCU from simultaneously occupying any station while it is traveling

between two stations during the corresponding relocation time period. Constraints (53)-(60) define the MCU charging and energy dynamics. MCUs are allowed to recharge at any energy hub during operation rather than being required to return to a depot, which provides greater operational flexibility during prolonged disruptions. Constraints (53) and (54) allow MCU charging and discharging operations only when the MCU is physically located at a charging station, limited by the corresponding charging and discharging power capacities. Constraint (55) ensures that residual charging demand is either served by MCUs or counted as unmet demand. Constraints (56) and (57) initialize and maintain MCU battery SOC requirements. The MCU traction energy used for relocation and the energy used to provide mobile charging service are represented through a single aggregated onboard battery energy state. Constraint (58) models MCU battery energy dynamics considering charging, discharging, and relocation energy consumption. Finally, Constraints (59) and (60) prevent simultaneous MCU charging and discharging operations within the same time interval.

4. Data description

We evaluate the proposed multi-stage optimization framework on UTA's transit network. The analysis integrates three primary data sources. First, operational records from UTA provide bus arrival and departure times, along with stop locations, for a full day of service. This dataset serves as the basis for constructing daily BEB schedules and route coverage. Terminal dwell times are extracted to identify potential charging opportunities and determine the buses present at each station during each time period, which are subsequently used to estimate charging demand and charger requirements. Second, high-resolution solar PV data were collected, consisting

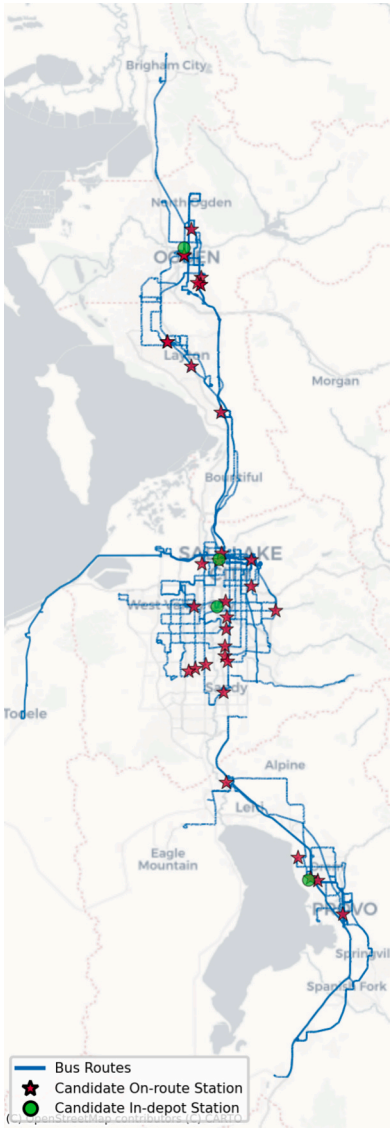


Fig. 2. Spatial layout of the bus network and candidate charging stations location.

of fifteen-minute interval solar irradiance measurements in 2023. These data capture both seasonal trends and intra-day fluctuations in solar energy potential. Data were obtained from the National Solar Radiation Database (NSRDB), which provides satellite-derived and model-generated solar irradiance values for each 4-km grid cell (Sengupta et al., 2018). For this study, we utilized data specific to the Salt Lake City area. Third, information on available rooftop area for each terminal station and garage is used to define the upper bounds for PV deployment, as shown in Fig. 12 of Appendix A. These spatial constraints are critical in determining how much solar infrastructure can be installed at each charging station, and thus influence both the system's energy generation and profitability. The geographic extent of the case study area is illustrated in Fig. 2, covering Box Elder, Weber, Davis, Tooele, Salt Lake, and Utah counties along the Wasatch Front region of Utah. Since short-trip buses do not require on-route charging, we focus on buses with long trip distances that exceed battery capacity and would need on-route charging after being replaced by BEBs. Next, we identify candidate on-route charging stations by selecting terminal stations where potential buses dwell for more than 10 minutes, ensuring sufficient time for potential on-route charging. All existing garages are selected as candidates to deploy in-depot charging stations.

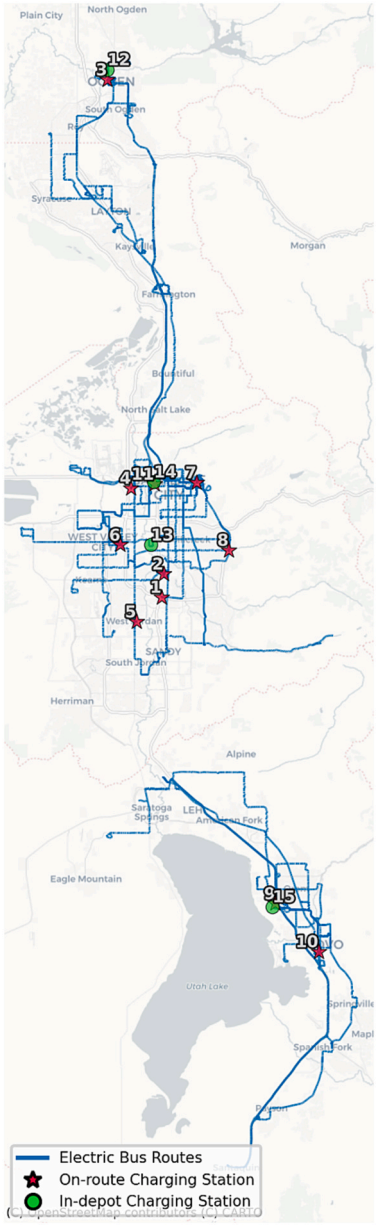


Fig. 3. Deployed BEB routes and selected charging station locations.

5. Results

We processed the data and formulated the model in Python. The optimization was performed using Gurobi, a commercial solver, on a computer with an Intel i5-8400 processor (2.80 GHz, 16 GB RAM, Windows 10). After full indexing, the proposed multi-stage model comprises approximately 784,261 decision variables, with 32,182 in Stage 1, 540,111 in Stage 2, and 211,968 in Stage 3. Stage 1 model was solved in approximately 8 minutes, while Stage 2 and 3 required approximately 40 and 30 minutes, respectively, all with an optimality gap below 5%. To manage the computational burden of the stochastic formulation, Stage 2 is decomposed into independent hub-level subproblems because no inter-hub coupling constraints are included. The seasonal representative-scenario approach also helps limit the problem size by avoiding the direct use of all historical daily PV profiles. Several parameter settings are provided in Appendix A. For Stage 1, according to UTA's zero-emission plan, a total of 156 buses are targeted for replacement with BEBs by 2035 (UTA, 2023). The solution finally replaces 156 conventional buses with BEBs, of which 115 require on-route charging. A total of 15 charging stations are selected: 11 on-route stations and 4 in-depot stations. The spatial distribution of deployed stations and BEB service routes is shown in Fig. 3. BEB service is primarily concentrated in Salt Lake City (central region) and Provo (southern region), with long corridors extending along the Salt Lake-Ogden axis. Based on the cost formulations in Equations (1)-(3), the total cost of electrification is approximately $179.88 million. Majority of this cost is attributable to bus replacement, which accounts for 84.1% ($151.32 million). In-depot charging stations contribute 8.8% ($15.90 million), on-route charging infrastructure 6.1% ($10.90 million), battery degradation cost 0.1% ($0.26 million), and MCU deployment 0.8% ($1.50 million).

Table 4 summarizes the deployment results for each charging station. On-route charging stations generally deploy one to four chargers, while in-depot stations require substantially more chargers to support overnight fleet charging. The total infrastructure cost increases with charger deployment scale. Results also reveal that the relationship between charger deployment, charging demand, and BEB coverage is not strictly proportional. Several stations, such as PROVFRST and ORANGEST, serve a relatively large number of BEBs despite moderate charging demand, suggesting that these stations primarily function as short-duration or fast-turnaround charging hubs. In contrast, stations such as OGNCENT and 39-SWASB exhibit comparatively high charging demand while serving fewer BEBs, indicating longer or more energy-intensive charging sessions per vehicle. Peripheral stations such as WVCNTRAX demonstrate relatively low utilization and primarily provide supplementary spatial coverage within the charging network. Such differences are important for robustness planning, as disruption impacts and MCU requirements may vary substantially across station types.

5.1. Schedule

In addition to deployment decisions, Stage 1 model also produces a station-level charging schedule based on discrete operational charging intervals. To better capture the detailed charging patterns and support the renewable energy operation analysis in Stage 2, the charging schedules are further converted into minute-level charging demand profiles. Fig. 4 illustrates the summed minute-by-minute charging demand throughout the day, separately for on-route and in-depot charging stations. The results show clear distinctions between on-route and in-depot stations in terms of charging patterns. In-depot stations mainly serve overnight charging demand and benefit from nighttime off-peak electricity prices. A small amount of daytime charging demand is also observed due to differences in route schedules and vehicle return times across the fleet. In contrast, on-route stations are more exposed to daytime peak electricity prices. These charging patterns provide the foundation for the Stage 2 energy hub optimization, where PV generation and energy storage can help reduce charging peak and improve operational profitability. Fig. 13 in Appendix C presents example charging schedules for selected stations.

5.2. Profit

Stage 2 converts each charging station into a renewable energy hub. Figs. 14–16 in the Appendix C show an example of the

Table 4
Station-level deployment results: chargers, BEBs served, and cost.

Station ID	Charging station	Number of chargers	Charging demand (KWh)	Charging infrastructure capital cost ($)	Number of served BEBs
1	FASHPLCE	1	1585	700,000	9
2	MURYCENT	1	2785	700,000	14
3	OGNCENT	1	2100	700,000	7
4	ORANGEST	1	1790	700,000	12
5	WJCTYCTR	1	2240	700,000	8
6	WVCNTRAX	1	1040	700,000	5
7	U.U.CTRL	1	2475	700,000	17
8	39-SWASB	2	3480	1,100,000	13
9	OREMFRST	3	6215	1,500,000	26
10	PROVFRST	3	7235	1,500,000	28
11	SLCSTATN	4	9165	1,900,000	27
12	Ogden Depot	6	3756	1,800,000	18
13	Meadowbrook Depot	13	9040	3,900,000	37
14	Central Depot	16	11,698	4,800,000	48
15	Orem Depot	18	11,565	5,400,000	53

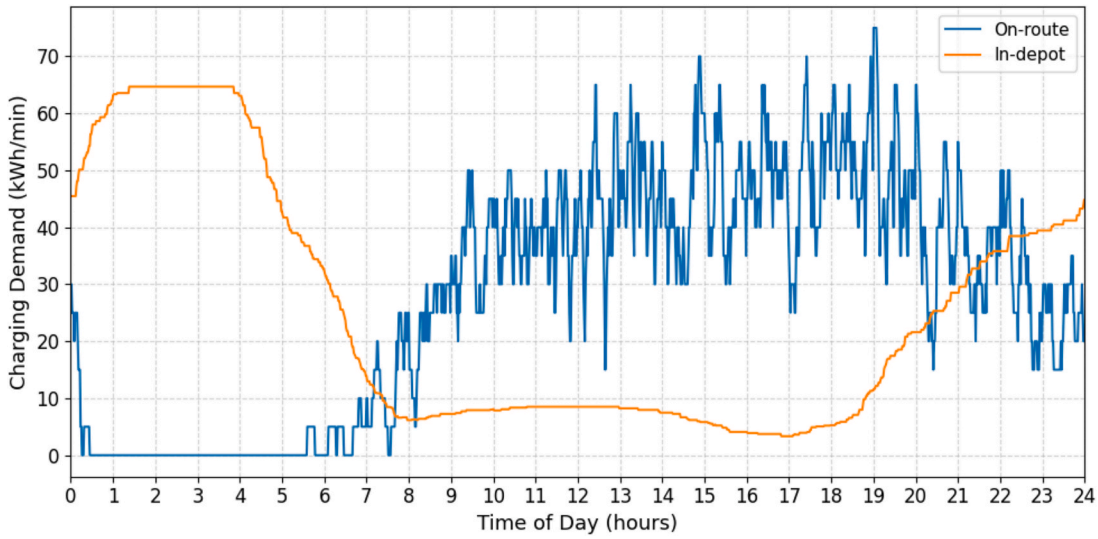


Fig. 4. Station-level temporal charging demand throughout the day.

optimized energy flows, including when to charge and discharge energy between the grid, solar PV, and storage throughout the day and the optimal timing and amount of energy to sell. Table 13 of Appendix B lists the PV selling prices for different time periods.

The deployment strategies and economic performance of each energy hub are evaluated using the stochastic optimization model developed in Stage 2, as shown in Fig. 5. One year of PV generation data is clustered into eight seasonal PV generation scenarios, as defined in Constraint (18). Figs. 5(a) and 5(b) present the optimal PV deployment areas and energy storage capacities under PV uncertainty. Based on the optimized infrastructure deployment, Fig. 5(c) shows the estimated seasonal profit of each energy hub calculated using the representative seasonal scenarios and their corresponding cluster sizes. Several important patterns can be observed. First, larger PV deployment areas generally lead to higher seasonal profits. For example, Meadowbrook Depot has the largest PV deployment area and achieves the highest profit. A similar trend is observed at high-demand on-route hubs such as SLCSTATN. Second, seasonal variation has a significant impact on system profitability. Most hubs generate substantially higher profits during summer due to increased solar generation, while winter profits decrease and become negative at several locations. In addition, charging demand influences profitability differently across hubs. Compared with Table 4, stations with high charging demand, such as SLCSTATN and Central Depot, experience larger seasonal profit fluctuations, while smaller stations with moderate demand, such as ORANGEST, exhibit more stable profit patterns throughout the year. The results suggest that maximizing PV deployment is not always economically optimal, particularly for hubs with high winter charging demand and limited seasonal solar generation.

We further calculate annual charging costs and net profits for each hub under two scenarios: with and without energy storage. The results are summarized in Table 5. Overall, energy storage significantly reduces charging costs and improves profitability at most on-route charging hubs. For example, charging costs at SLCSTATN decrease from $256,505 to $214,676, while ORANGEST and 39-SWASB shift from negative to positive annual profits after storage integration. These results indicate that energy storage effectively mitigates PV generation variability and reduces dependence on high-cost daytime electricity purchases. On the other hand, the benefits of energy storage remain limited at several on-route hubs. Although OREMFRST and PROVFRST experience noticeable charging cost reductions after storage integration, they still exhibit negative annual profits because of high charging demand (see Table 4) and limited PV deployment (see Fig. 5). A few on-route hubs, such as WJCTYCTR, even do not deploy energy storage. All in-depot hubs do not rely on energy storage while also achieve strong economic performance due to overnight charging patterns and large PV deployment areas. For example, Meadowbrook Depot generates the highest annual profit ($900,021).

To evaluate the long-term financial robustness of the energy hub system, we simulate the expected profit trajectories over a 10-year horizon. The PV deployment area and energy storage capacity determined are fixed over the planning horizon, while yearly operational profits are re-optimized under evolving system conditions. This analysis accounts for key trends, including projected increases in electricity prices, gradual declines in energy storage performance, and potential efficiency losses in PV generation. The results are shown in Fig. 6. Overall system profit remains positive and gradually decreases over time. On-route charging hubs remain unprofitable throughout the planning horizon, and their profit declines a bit faster because of higher dependence on daytime electricity purchases and limited renewable generation capacity. In contrast, in-depot charging hubs maintain relatively high and stable profits.

5.3. Resilience analysis of BEB system

We first evaluate the effectiveness of MCU deployment as backup charging resources. Fig. 7 illustrates the temporal utilization of fixed chargers and MCU activation across charging hubs obtained from Stage 1. The blue shading represents the number of occupied fixed chargers at each time period, while the gray outlines indicate periods when MCUs are deployed at the station. Referring to the number of chargers in Table 4, MCUs are activated only when all fixed chargers at a station are fully occupied. Therefore, MCU

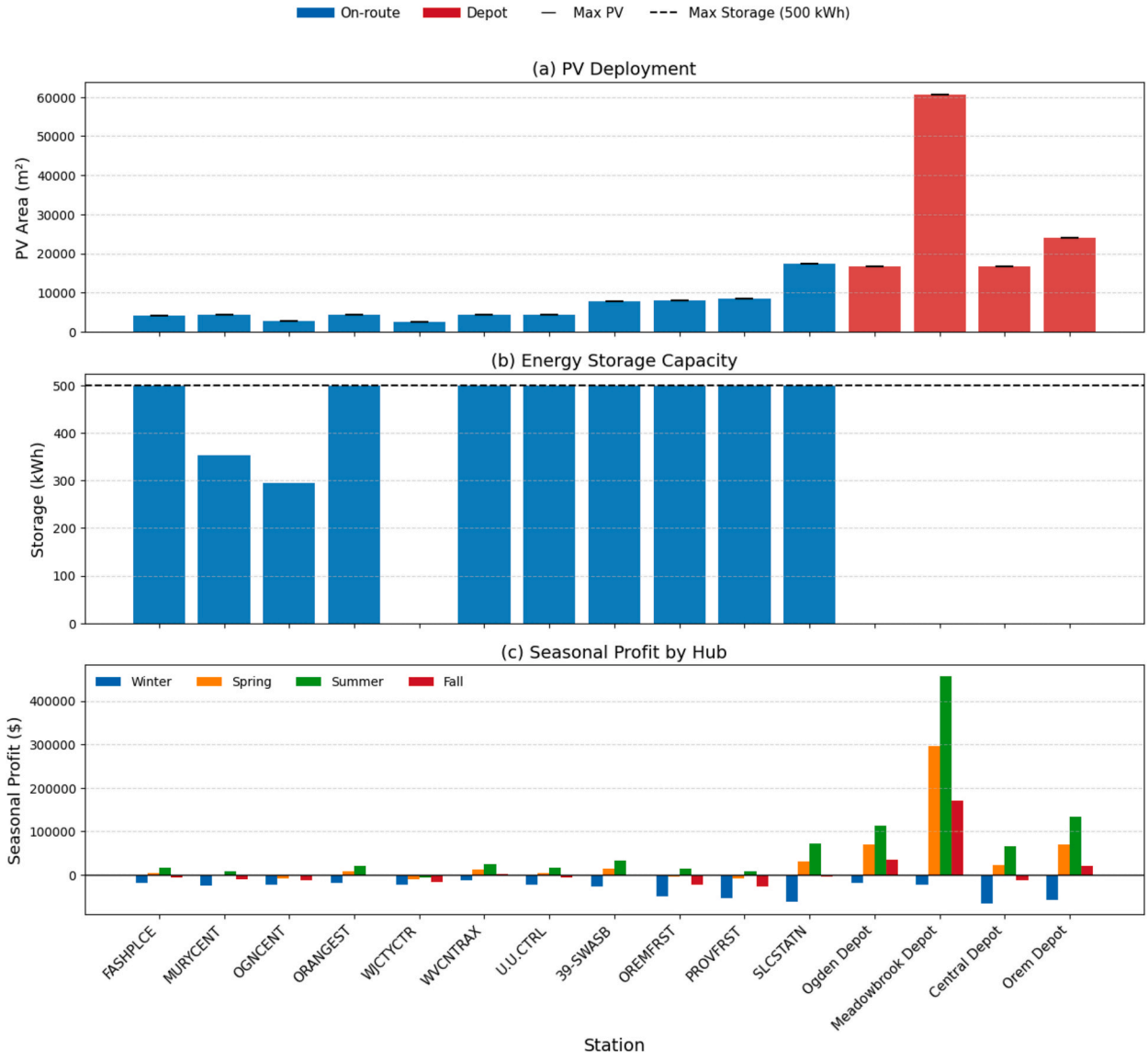


Fig. 5. Optimized renewable energy hub deployment and seasonal profit.

activation is highly targeted rather than continuously assigned to a single station, allowing a limited MCU fleet to dynamically support multiple charging hubs throughout the day. This operational flexibility enables the system to maintain high resilience with relatively low MCU deployment cost. The optimization results indicate that 10 MCUs are sufficient to provide full backup coverage for 11 charging hubs.

To verify the effectiveness of the MCU deployment in improving system resilience, actual MCUs operation under charger disruption scenarios is further evaluated. A peak-hour single-charger failure simulation is conducted for representative charging stations. Three representative station categories are selected to capture different operational characteristics. These include high-frequency stations with intensive charging activities, high-energy stations with large charging demand and peak loads, and typical stations with moderate charging utilization. For each station, the hour with the highest charging demand is identified as peak-hour, and one charger is assumed to fail for different durations during this period. Fig. 8 illustrates the baseline charging demand profile, deployed charger capacity, and the charging demand served by MCUs during the disruption period. The results show that MCUs can successfully provide backup charging when charger failures cause charging demand to exceed the remaining fixed charging capacity.

Table 6 summarizes the operational response from Stage 3 under representative peak-hour charger failure scenarios across different station categories. The residual demand column represents the original charging demand that cannot be served by fixed chargers because of charger failure or BEB arrival delay. As expected, residual demand generally increases with disruption duration. Typical station, i.e. U.U.CTRL with only one installed charger, experience higher residual demand during disruptions and require more MCU movements. MCU movements represent the number of inter-station MCU relocations required to provide sufficient backup charging.

Table 5
Annual profit comparison with and without energy storage.

Station ID	Energy hub	Annual charging cost ($)		Annual profit ($)	
		With storage	Without storage	With storage	Without storage
1	FASHPLCE	49,574	75,527	−4,653	−7,380
2	MURYCENT	88,957	105,983	−31,339	−34,755
3	OGNCENT	78,409	102,514	−46,216	−56,497
4	ORANGEST	33,551	68,642	6,917	−2,853
5	WJCTYCTR	–	95,389	–	−57,986
6	WVCNTRAX	32,579	66,322	24,790	10,181
7	U.U.CTRL	45,305	81,453	−8,722	−16,801
8	39-SWASB	89,127	123,977	15,566	−5,331
9	OREMFRST	158,610	206,351	−62,339	−92,820
10	PROVFRST	182,037	229,560	−81,516	−114,605
11	SLCSTATN	214,676	256,505	36,389	13,982
12	Ogden Depot	–	106,820	–	199,574
13	Meadowbrook Depot	–	232,624	–	900,021
14	Central Depot	–	291,699	–	8,964
15	Orem Depot	–	256,102	–	164,967

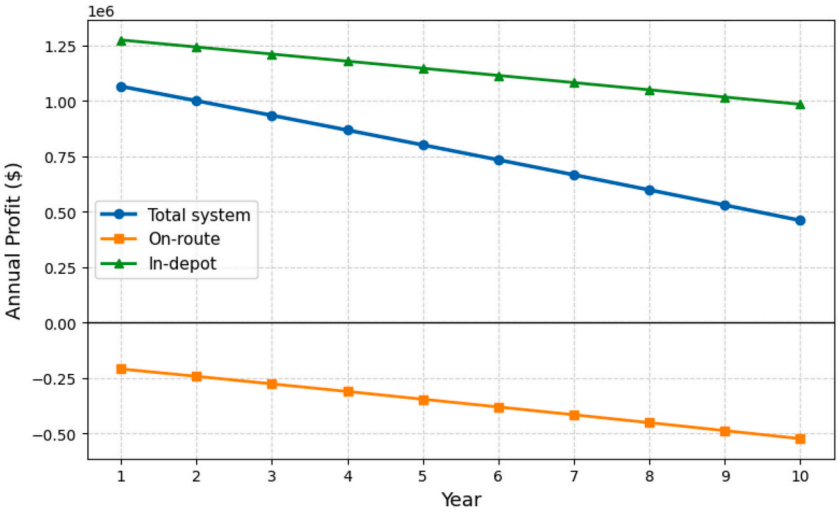


Fig. 6. Ten-year anticipated profit for in-depot and on-route charging hubs.

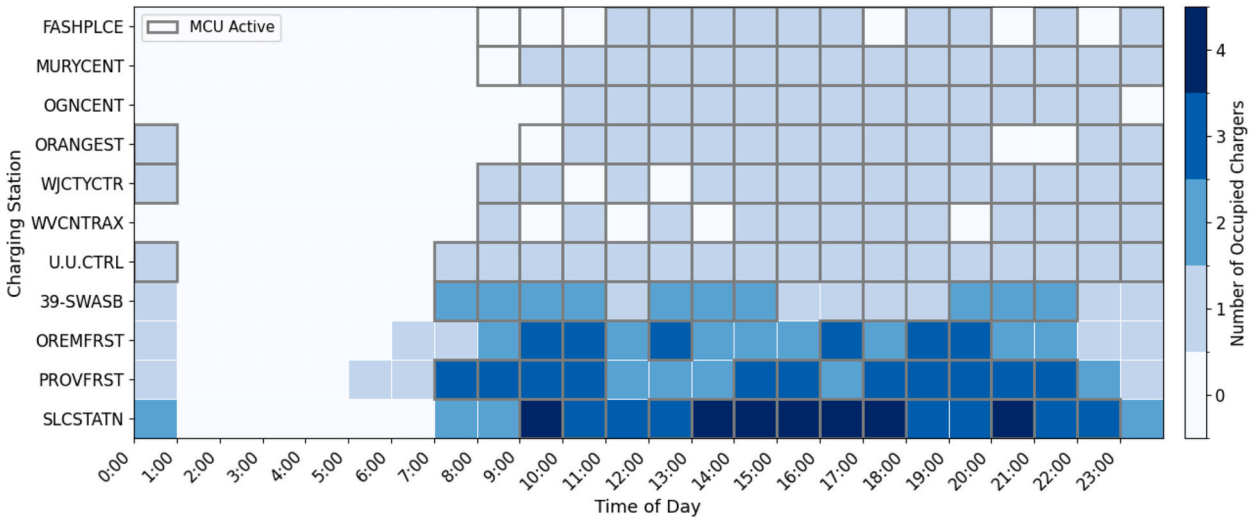


Fig. 7. MCU activation periods and corresponding charger occupancy.

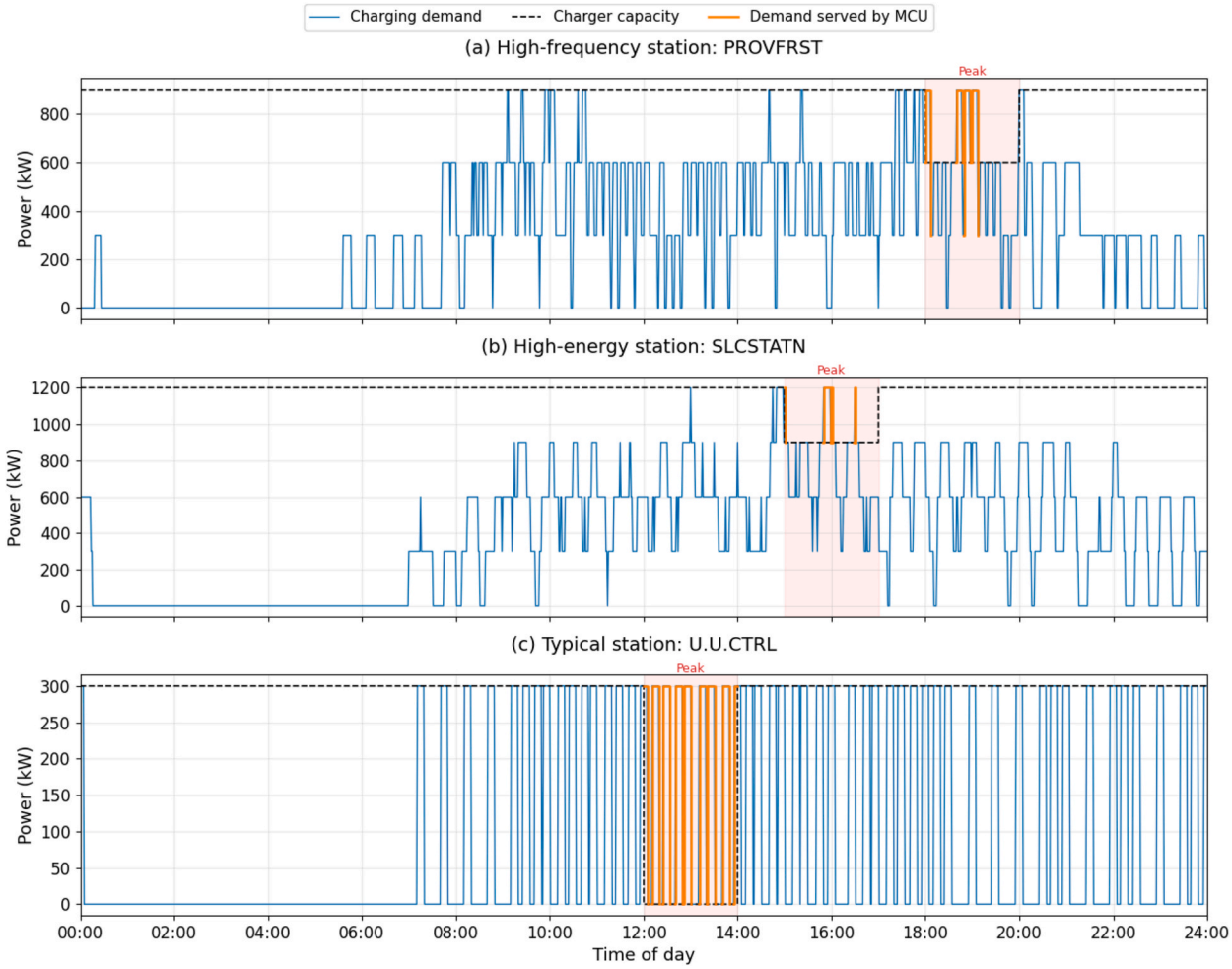


Fig. 8. MCU Response under peak-hour single-charger failure.

Table 6
Station-level operational response under peak-hour charger failures.

Scenario	Failure duration (min)	Residual demand (kWh)	Recovery rate (%)	MCU moves
High-frequency: PROVFRST	120	135	100	10
	180	170	100	10
	240	170	100	10
High-energy: SLCSTATN	120	60	100	10
	180	60	100	10
	240	60	100	10
Typical: U.U.CTRL	120	360	100	14
	180	560	100	16
	240	720	100	15

Under severe disruption conditions lasting from 2 to 4 hours, all residual charging demand is successfully served by MCUs, allowing the system to achieve full recovery without causing BEB service delays. These results demonstrate the effectiveness of MCUs in maintaining charging resilience during localized charger failures.

Finally, we evaluate the operational response under representative BEB line-delay scenarios. Similar to the station-failure analysis, representative disruptions are defined using high-frequency, high-energy, and typical bus lines during morning and afternoon peak periods, with different delay durations applied to affected BEB arrivals. Table 7 summarizes the residual demand, recovery rate, and MCU movements for each scenario. The results show that the proposed framework maintains nearly full recovery across most tested cases. MCUs successfully compensate for residual charging demand under high-energy and high-frequency line delays. Typical line during afternoon peak periods experience minor unmet demand under 30-minute delays but return to full recovery under longer

Table 7
Route-level impact of delay under different durations.

Scenario	Affected buses	Disruption window	Delay (min)	Residual demand (kWh)	Recovery rate (%)	MCU moves
High-energy line 217	10	08:00–10:00	30	150	100	11
			60	230	100	13
			120	170	100	11
		15:00–17:00	30	115	100	10
			60	120	100	10
			120	405	100	10
High-frequency line 33	15	08:00–10:00	30	195	100	10
			60	240	100	10
			120	235	100	11
		15:00–17:00	30	100	100	10
			60	200	100	10
			120	225	100	10
Typical line 35	15	08:00–10:00	30	100	100	10
			60	175	100	10
			120	185	100	10
		15:00–17:00	30	100	97.5	10
			60	100	100	10
			120	120	100	10

delays. This indicates that disruption impacts are not linearly related to delay duration, but also depend on jointly MCU support, the original BEB schedule, and fixed charger availability. In some cases, long-delayed BEB arrivals do not affect charging activities because sufficient charger capacity remains available. Compared with station-failure scenarios, line delays produce more variable residual demand patterns, reflecting the sensitivity of charging demand to BEB schedule disruptions. In contrast, MCU movement requirements remain relatively stable, indicating that line-delay recovery generally requires less MCU relocation effort.

5.4. *Sensitivity analysis*

A sensitivity analysis is conducted to evaluate the robustness of the proposed multi-stage optimization framework. Since different parameters affect different stages of the model, the analysis is performed separately for each stage using a tornado-diagram-based approach. Low and high parameter levels (±20% of the baseline value) are tested while keeping all other parameters fixed.

In Stage 1, the analysis focuses on deployment-related parameters affecting BEB infrastructure planning. The total deployment cost is selected as the performance metric. Fig. 9 shows that higher values of the BEB energy consumption rate lead to the largest increase in deployment cost, followed by in-depot charger cost, MCU unit cost, and first on-route charger cost. This indicates that vehicle energy performance and major infrastructure investments are the dominant factors in Stage 1 planning decisions. Some parameters exhibit non-monotonic behavior. For example, battery degradation-related parameters, including battery cost and cycle life, and additional on-route charger cost result in higher deployment costs under both low and high settings. This suggests that the baseline configuration is close to a balanced operating point, where deviations require additional infrastructure or operational adjustments.

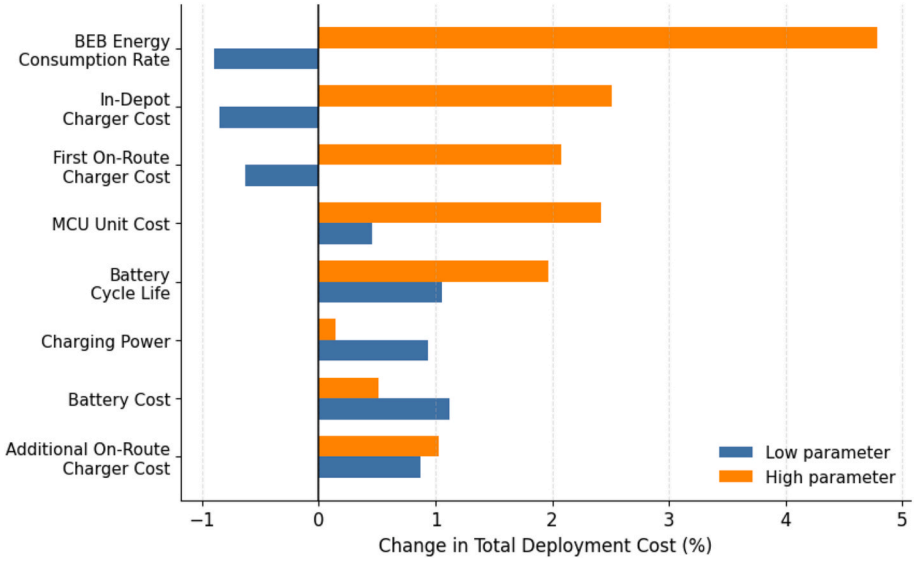


Fig. 9. Stage 1 sensitivity analysis of deployment cost.

In Stage 2, the analysis focuses on parameters affecting renewable energy hub performance, with annual net profit selected as the primary performance metric. Fig. 10 shows that PV-related parameters have the greatest impact on system profitability. PV output level and PV export price are the most sensitive factors, indicating that energy-hub performance strongly depends on solar generation conditions and electricity market value. PV installation cost and electricity purchase price also noticeably affect annual profit, while storage cost and efficiency have relatively smaller impacts, suggesting that energy storage mainly improves operational flexibility rather than acting as the primary economic driver.

Fig. 11 presents the sensitivity of Stage 3 recovery performance under the most severe station-failure and line-delay scenarios from Section 5.3, including a 240-minute charger failure and a 120-minute line delay. The results indicate that increased MCU travel time greatly reduces recovery performance. MCU availability also plays a critical role, particularly under line-delay disruptions. Those two parameters indicate that long travel time and a smaller MCU fleet reduce routing flexibility and timely charging support. MCU battery capacity has negligible impact on recovery performance within the tested ranges. Station-failure scenarios are more sensitive to MCU movement energy. Overall, the results demonstrate that operational accessibility and deployment flexibility of MCUs are more influential than energy-related parameters in maintaining charging resilience during disruptions.

6. Discussion

The proposed framework solves infrastructure deployment, renewable energy hub planning, and MCUs operations sequentially. This structure may partially separate the trade-offs between Stage 1 deployment decisions and the long-term renewable energy value evaluated in Stage 2, potentially introducing suboptimality. Specifically, charging stations with relatively high deployment costs in Stage 1 may be excluded despite having strong long-term renewable energy profit potential in Stage 2. To further investigate this issue, an additional analysis is conducted by incorporating a lifecycle PV economic-potential reward into the Stage 1 objective function:

$$min C^{S1} - \lambda^{PV} \sum_{n \in \mathcal{N}} B_n^{PV} Y_n \tag{61}$$

where C^{S1} is the original Stage 1 objective, $\mathcal{N} = \mathcal{J} \cup \mathcal{G}$ represents the candidate on-route and in-depot charging hubs, B_n^{PV} is the estimated lifecycle PV economic potential of hub n, Y_n represents its corresponding selection status, and λ^{PV} is a dimensionless weighting parameter controlling the contribution of long-term PV potential. To make the PV reward economically comparable with the Stage 1 deployment cost, B_n^{PV} is expressed directly as a discounted lifecycle monetary value. For each candidate hub, the PV economic potential is estimated as:

$$B_n^{PV} = \max\left\{0, \sum_{y=1}^{L^{PV}} \frac{N^{day}\left[E_{n,y}^{self}\bar{\lambda}_n^{buy} + E_{n,y}^{sell}\bar{\lambda}_n - c^{PV}y_n^{PV}\right]}{(1+r)^y}\right\} \tag{62}$$

where $E_{n,y}^{self}$ and $E_{n,y}^{sell}$ represent the estimated daily PV electricity used locally and exported to the grid at hub n in year y, respectively; $\bar{\lambda}_n^{buy}$ represents the corresponding average electricity purchase price; and $\bar{\lambda}_n$ is the PV selling price. L^{PV} is the PV system lifetime, and the discount rate is $r = 5\%$. This formulation gives higher priority to hubs with both high solar potential and high charging demand, while

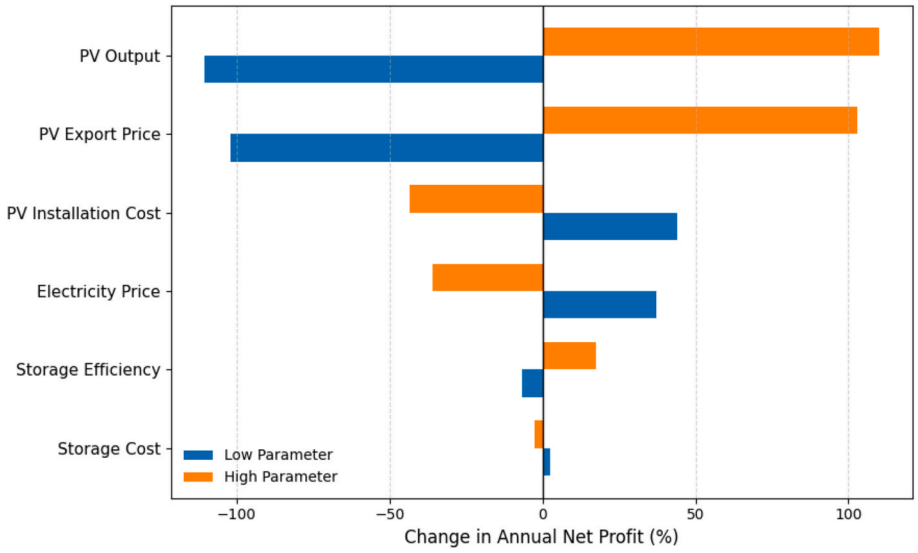


Fig. 10. Stage 2 sensitivity analysis of net profit.

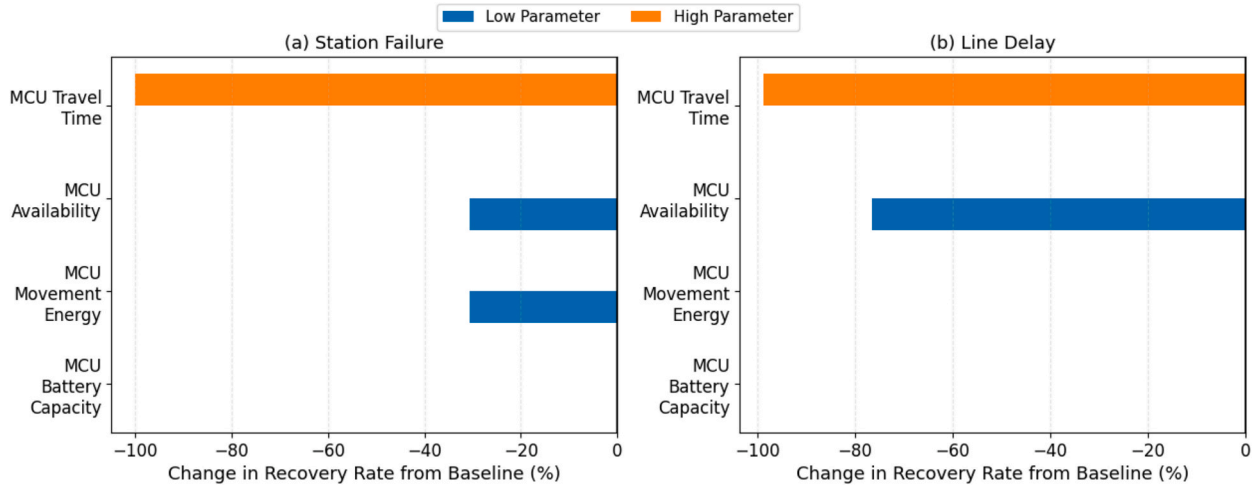


Fig. 11. Stage 3 sensitivity analysis of recovery rate.

high-solar but low-demand hubs receive a lower benefit because excess PV is valued at the selling price. Hubs with low solar potential receive limited benefits even with high charging demand, and hubs with both low solar potential and low demand receive the lowest or no PV reward.

As λ^{PV} is dimensionless, different values are tested to examine how strongly long-term PV economic potential influences Stage 1 deployment decisions. Table 8 presents representative sensitivity results. As λ^{PV} increases, the model generally shifts toward configurations with greater lifecycle PV potential. After $\lambda^{PV} = 0.4$, the improvement becomes marginal: increasing the multiplier to 0.7 provides no additional PV benefit while deployment cost increases. The PV potential reaches its maximum at $\lambda^{PV} = 1.0$ and then remains unchanged, while the number of selected energy hubs begins to decrease or fluctuate, indicating that the feasible PV potential has reached a saturation level.

In the Stage 2 model, electricity purchasing cost is calculated using the utility-specific billing structures adopted by the local electricity provider. However, some transit agencies may instead adopt simplified time-based TOU pricing schemes. To evaluate the flexibility of the proposed framework under different electricity pricing mechanisms, an alternative TOU-based billing formulation is introduced:

$$C_j^s = \sum_{t \in \mathscr{T}} \pi_{j,t} G_{j,t}^s \Delta_t \qquad \forall j \in \mathscr{J}^B, \forall s \in \Omega \tag{63}$$

$$\pi_{j,t} = \begin{cases} \pi_j^{\text{peak}}, & t \in \mathscr{T}^{\text{peak}} \\ \pi_j^{\text{off}}, & t \in \mathscr{T}^{\text{off}} \end{cases} \tag{64}$$

where C_j^s denotes the electricity purchasing cost at charging hub j under scenario s, $\pi_{j,t}$ is the TOU electricity price at time interval t, taking values of π_j^{peak} during peak periods $\left(t \in \mathscr{T}^{\text{peak}}\right)$ and π_j^{off} during off-peak periods $(t \in \mathscr{T}^{\text{off}})$, $G_{j,t}^s$ is the grid electricity purchase, and Δ_t is the duration of each time interval. This formulation replaces the electricity billing constraints in Equation (23)-(32) while preserving the remaining optimization framework. The TOU pricing parameters are summarized in Table 14 in Appendix B.

Table 9 compares the Stage 2 optimization results under the original utility-specific billing structure and the alternative time-based TOU billing structure. The results show that the TOU formulation significantly improves overall system profitability while reducing the optimal energy storage capacity. This is mainly because the time-based TOU structure removes demand-related charges and block-rate penalties, reducing the need for large storage systems for peak shaving. The total PV deployment area and the number of selected energy hubs remain unchanged, indicating that the proposed framework can maintain stable renewable-energy deployment decisions

Table 8
Impact of PV-potential reward.

PV multiplier λ^{PV}	Stage 1 deployment cost ($)	Net lifecycle PV potential ($)	Number of energy hubs
0.0	1.79E + 08	4.87E + 07	15
0.2	1.81E + 08	5.10E + 07	18
0.4	1.83E + 08	5.36E + 07	21
0.7	1.86E + 08	5.36E + 07	23
1.0	1.88E + 08	5.54E + 07	26
2.0	1.85E + 08	5.54E + 07	24

Table 9
Comparison of original and TOU billing structures.

Billing structure	Total Expected daily profit ($)	Total PV area (m^2)	Total storage capacity (kWh)	Number of energy hubs
Original billing structure	2,865	186,850	4,648	15
Time-based TOU billing	4,979	186,850	2,229	15

under different electricity pricing mechanisms.

The proposed framework adopts different temporal resolutions across the three stages according to their planning objectives. Stage 1 uses stop-sequence and 15-minute charging occupancy for BEBs and 20-minute activation intervals for MCUs to support infrastructure and backup planning. Stage 2 uses minute-level charging demand profiles for renewable energy and storage operation, while Stage 3 adopts 20-minute intervals for detailed MCU scheduling. To connect these temporal resolutions, the charging schedule determined in Stage 1 is first converted into a minute-level charging demand profile based on the fixed charging power and charging duration. This minute-level profile provides a common representation of charging demand for the subsequent stages and can be directly used or aggregated into different time intervals according to the needs of each stage.

This flexible temporal-resolution strategy is particularly suitable for planning and decision support. Stage 1 provides charging demand and charging duration requirements that can be used to accommodate charging activities within available dwell times. Stage 2 provides energy management strategies for renewable energy utilization, battery charging and discharging, and grid energy exchange. Stage 3 determines MCU deployment and relocation strategies, enabling agencies to establish response plans for charger failures and prolonged BEB delays. Future research may integrate rolling-horizon optimization and real-time control strategies to further enhance operational adaptability.

7. Conclusion

This study developed a multi-stage optimization framework to guide the transition of conventional bus fleets to a BEB system, support their integration with renewable energy, and prevent potential operation disruptions. Stage 1 minimizes total deployment cost while ensuring operational robustness. A key contribution is the explicit modeling of in-depot charging activities, including station locations, capacities, and schedules. This stage also distinguishes between charger types with varying costs and introduces MCUs as flexible, off-grid backup resources to enhance system robustness in the face of travel delays or charger failures. Stage 2 transforms each charging station into a renewable energy hub by optimizing solar PV generation and battery storage usage to reduce grid dependency and maximize economic performance under stochastic solar conditions. A key highlight is the stochastic optimization framework that captures seasonal PV variability across both on-route and in-depot charging hubs. The third stage develops real-time MCU dispatch and relocation strategies to maintain charging service continuity under charger disruptions and bus operation delays. Additionally, comprehensive sensitivity analyses across different stages further demonstrate the robustness of the proposed framework and identify the key factors influencing deployment cost, renewable energy profitability, and operational resilience.

The model was applied to a city-scale public transit network operated by the UTA. A total of 156 buses were replaced with BEBs, supported by 11 on-route and 4 in-depot charging stations. The results reveal distinct functional roles among stations, some serve as high-turnover transfer points, while others act as terminal or overnight hubs. Charging patterns vary accordingly and are incorporated into Stage 2, where they influence both electricity costs and the alignment with PV generation. The integration of PV and battery storage enables all renewable energy hubs to offset the original charging costs, with most hubs achieving positive profits during summer months. However, due to seasonal solar fluctuations, only a few on-route charging hubs maintain profitability throughout the year. Energy storage significantly enhances profit stability, particularly for on-route charging hubs, while it is less critical for in-depot hubs whose operations already align with off-peak grid pricing. The economic value of PV and storage depends on hub characteristics, including hub type (e.g., on-route vs. in-depot), operational scale (e.g., PV deployment and charging demand), and seasonal conditions (e.g., summer vs. winter). Notably, higher annual profits are often accompanied by greater seasonal variability. Operational robustness analysis confirms that MCUs effectively mitigate disruptions caused by charger failures and arrival delays, thereby improving overall BEB system resilience. Sensitivity analysis indicates that BEB energy consumption and major infrastructure investment costs are the dominant factors affecting deployment decisions, while electricity pricing structures and PV-related parameters strongly influence long-term energy-hub profitability. Additional analyses further show that incorporating lifecycle PV economic potential into Stage 1 can increase long-term renewable energy value, but this improvement is accompanied by higher deployment costs and eventually reaches a saturation level as the weighting parameter increases. Moreover, comparisons between the original utility-specific billing structure and an alternative time-based TOU pricing scheme reveal that electricity pricing mechanisms can substantially affect optimal storage sizing and overall system profitability.

Future work may extend the model by incorporating labor and maintenance costs, particularly relevant in emerging renewable energy hubs. Further research could explore trade-offs between cost and operational robustness, as well as assess the sensitivity of PV and storage efficiency parameters on long-term investment strategies. In addition, the current Stage 2 treats PV generation uncertainty and transit-side operational variations independently. In reality, lower PV generation may be associated with adverse weather conditions, especially during extreme weather events, which can also increase BEB energy consumption and disrupt charging schedules. These simultaneous changes on the supply and demand sides could create more severe system impacts than those represented in the current model. Future studies could therefore incorporate joint weather-traffic-energy uncertainty scenarios to better capture these coupled effects. Regarding MCU deployment, this study only considers scenarios where one charger serves as a backup. Future

extensions could examine more complex conditions, such as multiple charger failures or increased occurrences of delayed BEB arrivals, to better inform investment decisions for MCU allocation. The charging activities of MCUs and their potential role as mobile energy carriers facilitating energy transfer between the grid and charging hubs also warrant further investigation.

CRediT authorship contribution statement

Shouzheng Pan: Writing – original draft, Methodology, Formal analysis, Data curation, Conceptualization. **Xiaohan Liu:** Methodology, Formal analysis, Conceptualization. **Xiaoyue Cathy Liu:** Writing – review & editing, Project administration, Methodology, Funding acquisition, Conceptualization. **Xiaolei Ma:** Methodology, Formal analysis, Conceptualization. **Ran Wei:** Methodology, Formal analysis.

Declaration of Competing Interest

The authors declare that they have no known competing financial interests or personal relationships that could have appeared to influence the work reported in this paper.

Appendix A. . Parameter settings

Table 10 presents the detailed parameter settings used in both Stage 1 and Stage 2, based on existing research.

Table 10
Parameter settings for Stage 1 and Stage 2.

Parameters	Values
Capital cost per BEB unit	$ 970,000
Capital cost of first on-route charger	$ 700,000
Capital cost of subsequent on-route charger (per unit)	$ 400,000
Capital cost of in-depot charger (per unit)	$ 300,000
Capital cost of MCU (per unit)	$ 150,000
Capacity per on-route charger	1
Capacity per in-depot charger	3
Energy efficiency	3 kWh/mile
Full BEB battery capacity	388 kWh
On-route charger power capacity	300 kW
Energy storage efficiency	90%
Max energy storage capacity	500 kWh
Daily energy storage cost	0.08 $/kwh
Daily solar PV cost	0.034 $/$m^2$
Energy storage lifetime	10 years
Solar PV lifetime	25 years
Storage C-rate	0.6
Battery service life	5 years
Operating days per year	250 days/year
Battery replacement cost	$100/kWh
Battery cycle life	4000
Usable depth of discharge	0.6
Degradation weighting factor	0-1
Battery degradation cost coefficient	0.1

Fig. 12 illustrates the allowable PV development area for each charging station based on actual geomatic conditions. In-depot charging stations generally have significantly larger available areas for PV deployment compared to on-route charging stations. Among them, Meadowbrook depot possesses the largest development area, resulting in the highest potential for profit generation.

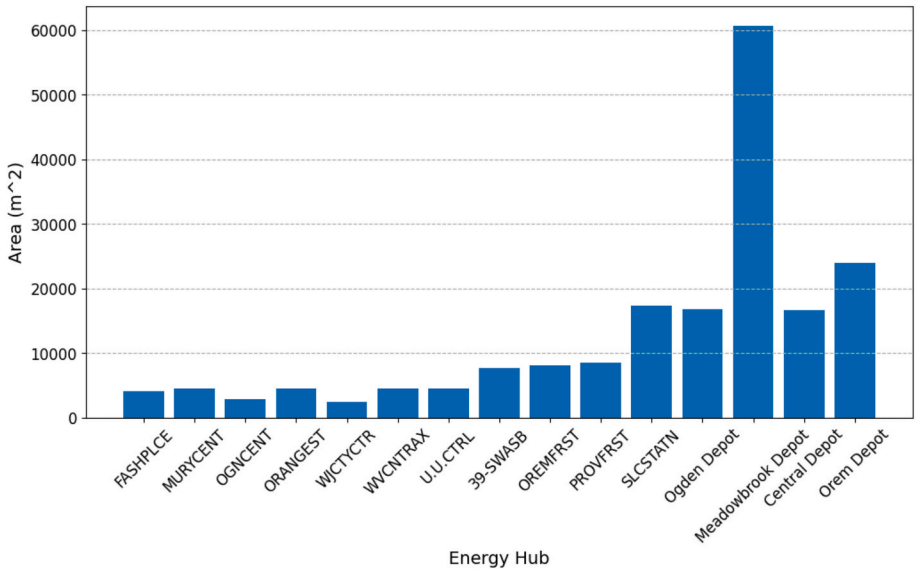


Fig. 12. Max allowable PV area for each charging station.

Appendix B. . Electricity prices policy

Table 11 presents the charging rate policy for on-route charging stations, based on the tariff structure provided by Rocky Mountain Power for UTA. Table 12 outlines the corresponding charging rate policy applied to in-depot charging stations. Table 13 presents the time-of-use feed-in tariffs used for exported PV electricity. Table 14 lists TOU pricing parameters which are designed based on representative tariffs from Rocky Mountain Power (RMP, 2025)

Table 11
Tariff structure under billing policy 1.

Item	Summer (April to October)	Winter
Basic charge	$ 53	$ 53
First 50 kWh/kW	0.2815 $/kWh	0.2491 $/kWh
All additional kWh	0.1030 $/kWh	0.0912 $/kWh
Off-peak kWh	-0.0833 $/kWh	-0.0737 $/kWh

Table 12
Tariff structure under billing policy 2.

Item	Summer (April to October)	Winter
Basic charge	$ 10	$ 10
First 1500 kWh	0.1171 $/kWh	0.1036 $/kWh
All additional kWh	0.0655 $/kWh	0.0580 $/kWh

Table 13
Feed-in tariff for exported PV electricity.

Period	Feed-in tariff / grid value of exported PV ($/kWh)
Off-peak	0.03
Mid-peak	0.05
On-peak	0.12

Table 14
TOU electricity pricing structure.

Station type	Season	Peak period	Off-peak period	Peak price ($/kWh)	Off-peak price ($/kWh)
On-route	Summer, Jun-Sep	3:00 PM–10:00 PM	Other hours	0.17	0.05
	Non-summer, Oct-May	6:00 AM–9:00 AM; 6:00 PM–10:00 PM	Other hours	0.14	0.045
In-depot	Summer, Jun-Sep	3:00 PM–10:00 PM	Other hours	0.12	0.04
	Non-summer, Oct-May	6:00 AM–9:00 AM; 6:00 PM–10:00 PM	Other hours	0.10	0.035

Appendix C. . Examples of charging schedule, energy flow

Fig. 13 presents the charging schedules for the SLCSTATN on-route charging station and the Orem in-depot charging station. The charging peak at SLCSTATN occurs between 9:00 a.m. and 10:00 p.m., while the Orem depot experiences higher peak charging demand between 1:00 a.m. and 4:00 a.m., with an additional increase in demand from 11:00 a.m. to 2:00 p.m.

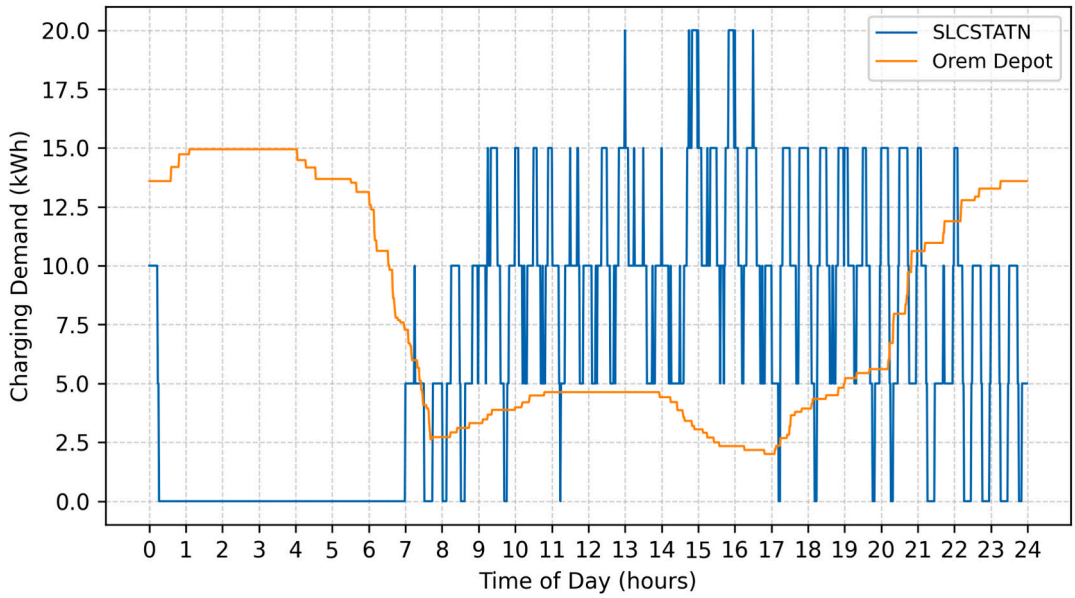


Fig. 13. Charging schedule of SLCSTATN and Orem depot charging station.

Fig. 14 presents the minute-level energy flows from solar PV generation alongside the actual BEB charging demand for a representative day in June at U.U.CTRL hub. As shown, total solar PV generation consistently exceeds BEB charging demand before approximately 6:00 p.m. During periods with active BEB charging, solar energy is prioritized for direct vehicle charging. At other times, surplus PV energy is either exported to the grid or stored in the battery system.

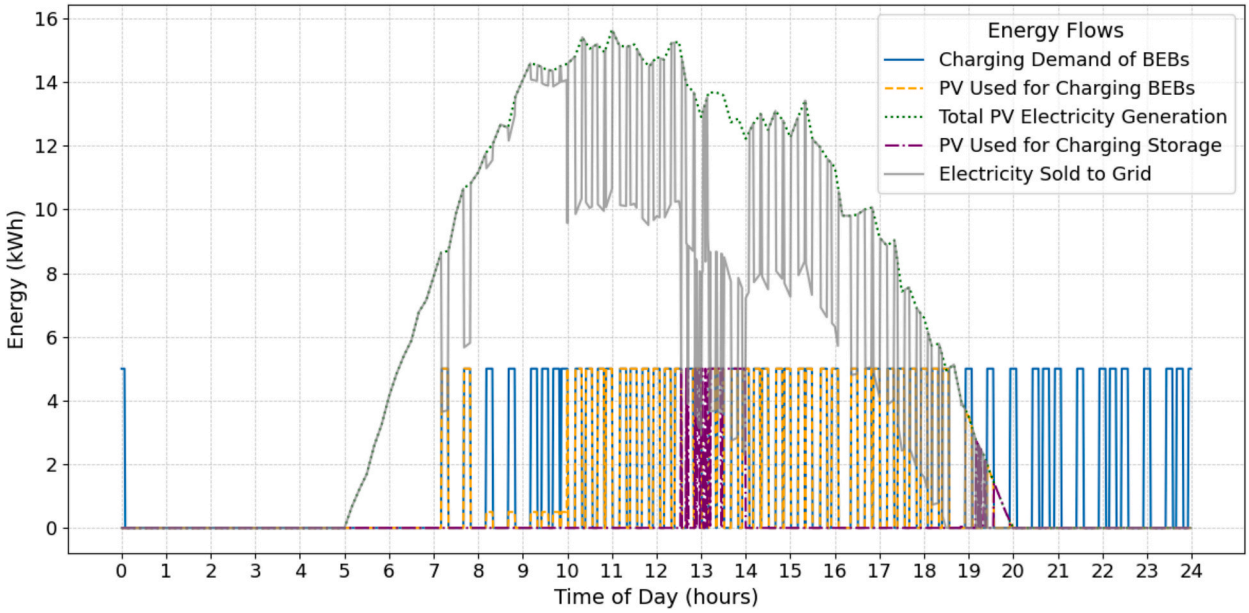
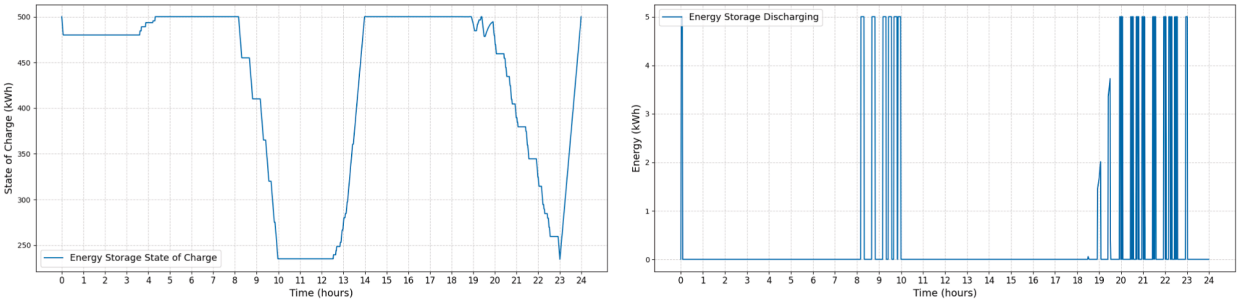


Fig. 14. Daily energy flow at U.U.CTRL energy hub.

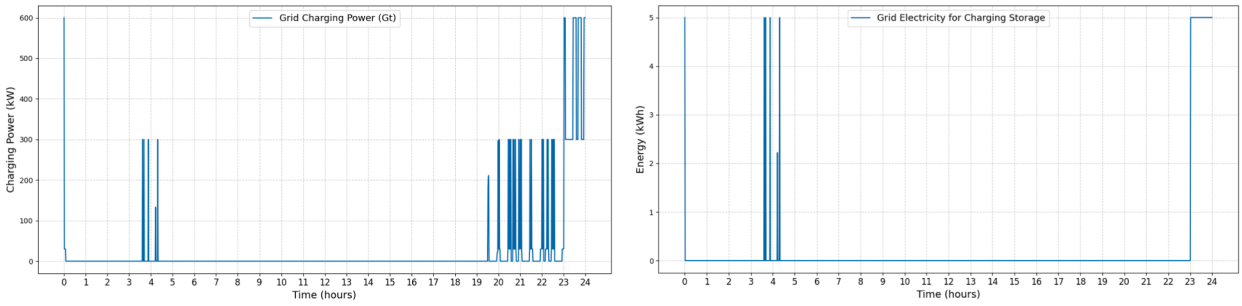
Fig. 15 presents the Energy Storage State of Charge and discharging state for U.U.CTRL hub. Decide by model, the best Discharging time and energy will be optimized to make sure the max profit. The use of storage mainly happen in 8 to 10 am, 19 to 23 pm, and 0 to 1 am.



(a) State of charge (b) Discharging profile

Fig. 15. Energy Storage State of Charge and discharging profile at U.U.CTRL energy hub.

Fig. 16 presents the grid-supplied charging power to BEBs and the energy used to charge storage at the U.U.CTRL energy hub. Compared to Stage 1, where BEBs rely solely on the grid for charging, the energy hub stage significantly reduces grid dependence. Grid charging primarily occurs after 8:00 p.m., when solar PV generation ceases, while storage charging from the grid takes place mainly around midnight. This optimized schedule effectively avoids peak daytime grid usage and maximizes the utilization of solar PV to enhance overall profitability.



(a) Charging power supplied to BEBs (b) Energy allocated to storage charging

Fig. 16. Grid-supplied energy at the U.U.CTRL energy hub.

Data availability

Data will be made available on request.

References

Afshar, S., Pecenak, Z.K., Barati, M., Disfani, V., 2022. Mobile charging stations for EV charging management in urban areas: A case study in Chattanooga. Appl. Energy 325, 119901.

An, K., 2020. Battery electric bus infrastructure planning under demand uncertainty. Transp. Res. Part C Emerging Technol. 111, 572–587.

Atlas Public Policy, 2023. Colorado State Fleet Electricity Rate Analysis. Available at: https://atlaspolicy.com/wp-content/uploads/2023/03/Colorado-State-Fleet-Electricity-Rate-Analysis-1.pdf (Accessed: 5 August 2026).

Bao, Z., Li, J., Bai, X., Xie, C., Chen, Z., Xu, M., Shang, W.L., Li, H., 2023. An optimal charging scheduling model and algorithm for electric buses. Appl. Energy 332, 120512.

Bazarnovi, S., Cokyasar, T., Verbas, O., Mohammadian, A.K., 2025. Optimizing charging infrastructure for battery electric buses: A stochastic location model with budget constraints. Procedia Comput. Sci. 257, 583–590.

California Air Resources Board (CARB), 2022. Electricity Costs for Battery Electric Bus Operation. Available at: https://ww2.arb.ca.gov/sites/default/files/2022-06/ratesanddemand_ADA.pdf (Accessed: 5 August 2026).

Can, C., Kilic, F., Kaya, Y., 2025. A novel approach for location planning of fast-charging stations for e-buses. International Journal of Simulation Modelling (IJSIMM) 24 (2), 213–224.

Chen, B., Chen, Z., Liu, X.C., Zheng, N., Xiao, Q., 2024. Measuring the effectiveness of incorporating mobile charging services into urban electric vehicle charging network: An agent-based approach. Renew. Energy 234, 121246.

Chen, Q., Niu, C., Tu, R., Li, T., Wang, A., He, D., 2023. Cost-effective electric bus resource assignment based on optimized charging and decision robustness. Transp. Res. Part D: Transp. Environ. 118, 103724.

Cokyasar, T., Verbas, O., Auld, J., 2023. Electric vehicle scheduling problem with tour combinations. Procedia Comput. Sci. 220, 413–420.

Davatgari, A., Cokyasar, T., Verbas, O., Mohammadian, A.K., 2024. Heuristic solutions to the single depot electric vehicle scheduling problem with next day operability constraints. Transp. Res. Part C Emerging Technol. 163, 104656.

Dirks, N., Schiffer, M., Walther, G., 2022. On the integration of battery electric buses into urban bus networks. Transp. Res. Part C Emerging Technol. 139, 103628.

Duan, S., Zhang, Z., Wang, Z., Xiong, X., Chen, X., Que, X., 2025. A study on mobile charging station combined with integrated energy system: Emphasis on energy dispatch strategy and multi-scenario analysis. Renew. Energy 239, 122111.

Fan, D., Wang, Y., Bai, X., Liu, Y., 2025. Sustainable planning battery electric buses charging station under two decision-making criteria. J. Ind. Inf. Integr., 100937

Foda, A., Mohamed, M., Farag, H., El-Saadany, E., 2023. A resilient battery electric bus transit system configuration. Nat. Commun. 14 (1), 8279.

Godfrey, J. and Sipiora, A., 2023. Procuring and Maintaining Battery Electric Buses and Charging Systems–Best Practices (No. FTA Report No. 0253). United States. Department of Transportation. Federal Transit Administration.

He, J., Yan, N., Zhang, J., Wang, T., Chen, Y.Y., Tang, T.Q., 2023a. Battery electricity bus charging schedule considering bus journey's energy consumption estimation. Transp. Res. Part D: Transp. Environ. 115, 103587.

He, Y., Liu, Z., Song, Z., 2022. Integrated charging infrastructure planning and charging scheduling for battery electric bus systems. Transp. Res. Part D: Transp. Environ. 111, 103437.

He, Y., Liu, Z., Song, Z., 2023c. Joint optimization of electric bus charging infrastructure, vehicle scheduling, and charging management. Transp. Res. Part D: Transp. Environ. 117, 103653.

He, Y., Liu, Z., Zhang, Y., Song, Z., 2023b. Time-dependent electric bus and charging station deployment problem. Energy 282, 128227.

He, Y., Song, Z., Liu, Z., 2019. Fast-charging station deployment for battery electric bus systems considering electricity demand charges. Sustain. Cities Soc. 48, 101530.

Institute for Transportation and Development Policy (ITDP), 2018. China Tackles Climate Change with Electric Buses. Available at: https://itdp.org/2018/09/11/electric-buses-china/ (Accessed: 5 August 2026).

Islam, S.M.M., Salema, A.A., Saleheen, M.Z., Lim, J.M.Y., 2022. The influence of shifting the electric bus charging routine on the techno-economic performance of a solar-powered bus depot. Energy 239, 122316.

Jeffers, M. and Eudy, L., 2021. Foothill Transit Battery Electric Bus Evaluation (No. NREL/TP-5400-80022). National Renewable Energy Lab.(NREL), Golden, CO (United States).

Johnson, C., Nobler, E., Eudy, L. and Jeffers, M., 2020. Financial analysis of battery electric transit buses (No. NREL/TP-5400-74832). National Renewable Energy Lab.(NREL), Golden, CO (United States).

Li, W., He, Y., Hu, S., He, Z., Ratti, C., 2024. Planning dynamic wireless charging infrastructure for battery electric bus systems with the joint optimization of charging scheduling. Transp. Res. Part C Emerging Technol. 159, 104469.

Lim, L.K., Ab Muis, Z., Ho, W.S., Hashim, H., Bong, C.P.C., 2023. Review of the energy forecasting and scheduling model for electric buses. Energy 263, 125773.

Liu, X., Liu, X.C., Xie, C., Ma, X., 2023. Impacts of photovoltaic and energy storage system adoption on public transport: a simulation-based optimization approach. Renew. Sustain. Energy Rev. 181, 113319.
Liu, X., Plötz, P., Yeh, S., Liu, Z., Liu, X.C., Ma, X., 2024. Transforming public transport depots into profitable energy hubs. Nat. Energy 9 (10), 1206–1219.
Liu, Z., Wang, X., Zhang, F., 2021. Full life-cycle optimal battery scheduling for maximal lifetime value considering degradation. IEEE Trans. Energy Convers. 37 (2), 1379–1393.
Mouli, G.C., Bauer, P., Zeman, M., 2016. System design for a solar powered electric vehicle charging station for workplaces. Appl. Energy 168, 434–443.
Najafi, A., Gao, K., Parishwad, O., Tsaousoglou, G., Jin, S., Yi, W., 2025. Integrated optimization of charging infrastructure, electric bus scheduling and energy systems. Transp. Res. Part D: Transp. Environ. 141, 104664.
Ozturk, Z., Demirci, A., Terkes, M., Yumurtaci, R., 2025. Optimal planning of solar PV-based electric vehicle charging stations empowered by energy storage system: Feasibility and green charge potential. Renew. Energy, 123715.
Ren, H., Ma, Z., Tse, C.F.N., Sun, Y., 2022. Optimal control of solar-powered electric bus networks with improved renewable energy on-site consumption and reduced grid dependence. Appl. Energy 323, 119643.
Rocky Mountain Power, 2025. Time of Day Pricing. Available at: https://www.rockymountainpower.net/savings-energy-choices/time-of-day.html (Accessed: 5 August 2026).
Rocky Mountain Power (RMP), 2024. Schedule 6A: General Service-Energy Time of Day Option. Available at: https://www.rockymountainpower.net/content/dam/pcorp/documents/en/rockymountainpower/rates-regulation/utah/rates/006A_General_Service_Energy_Time_of_Day_Option.pdf (Accessed: 5 August 2026).
Sengupta, M., Xie, Y., Lopez, A., Habte, A., Maclaurin, G., Shelby, J., 2018. The National Solar Radiation Database (NSRDB). Renew. Sustain. Energy Rev. 89, 51–60.
Sistig, H.M., Sinhuber, P., Rogge, M., Sauer, D.U., 2025. Evaluating costs and operations of public bus fleet electrification. npj Sustainable Mobility and Transport 2 (1), 15.
State Council of the People's Republic of China, 2024. Over 80 pct of China's buses powered by new energy. Available at: https://english.www.gov.cn/archive/statistics/202411/15/content_WS67370ec7c6d0868f4e8ed002.html (Accessed: 5 August 2026).
Tang, C., Shi, H., Liu, T., 2023. Optimization of single-line electric bus scheduling with skip-stop operation. Transp. Res. Part D: Transp. Environ. 117, 103652.
Tang, X., Lin, X., He, F., 2019. Robust scheduling strategies of electric buses under stochastic traffic conditions. Transp. Res. Part C Emerging Technol. 105, 163–182.
Utah Transit Authority (UTA), 2023. 2023 UTA Zero Emission Bus Transition Plan. Available at: https://rideuta.com/-/media/Files/About-UTA/Innovative-Mobility/2023_UTA_Zero_Emission_Bus_Transition_Plan.pdf (Accessed: 5 August 2026).
Wang, J., Kang, L., Liu, Y., 2020. Optimal scheduling for electric bus fleets based on dynamic programming approach by considering battery capacity fade. Renew. Sustain. Energy Rev. 130, 109978.
Wang, Z., Zheng, F., Hamdan, S., Jouini, O., 2025a. Charging scheduling optimisation of battery electric buses with charging setup time. Int. J. Prod. Res. 63 (10), 3538–3563.
Wang, Z., Zheng, F., Hamdan, S., Jouini, O., 2025b. On the spatio-temporal optimization for the charging scheduling of battery electric buses. Transportation Research Part E: Logistics and Transportation Review 197, 104086.
Wu, M., Yu, C., Ma, W., An, K., Zhong, Z., 2022. Joint optimization of timetabling, vehicle scheduling, and ride-matching in a flexible multi-type shuttle bus system. Transp. Res. Part C Emerging Technol. 139, 103657.
Ye, Z., Yu, N., Wei, R., Liu, X.C., 2022. Decarbonizing regional multi-model transportation system with shared electric charging hubs. Transp. Res. Part C Emerging Technol. 144, 103881.
Yi, Z., Chen, B., Liu, X.C., Wei, R., Chen, J., Chen, Z., 2023. An agent-based modeling approach for public charging demand estimation and charging station location optimization at urban scale. Comput. Environ. Urban Syst. 101, 101949.
Zhang, L., Liu, Z., Wang, W., Yu, B., 2022. Long-term charging infrastructure deployment and bus fleet transition considering seasonal differences. Transp. Res. Part D: Transp. Environ. 111, 103429.
Zhang, M., Yang, M., Zhao, J., 2025. Analysis of the Robustness of Electric Bus Networks under Disruptions. Transp. Res. Rec., 03611981251327196
Zhang, Y., Liu, X., Wei, W., Peng, T., Hong, G., Meng, C., 2020. Mobile charging: A novel charging system for electric vehicles in urban areas. Appl. Energy 278, 115648.
Zhao, J., Li, F., Zhang, Q., 2024. Impacts of renewable energy resources on the weather vulnerability of power systems. Nat. Energy 9 (11), 1407–1414.
Zhou, Y., Liu, X.C., Wei, R., Golub, A., 2020. Bi-objective optimization for battery electric bus deployment considering cost and environmental equity. IEEE Trans. Intell. Transp. Syst. 22 (4), 2487–2497.
Zhou, Y., Wang, H., Wang, Y., Li, R., 2022. Robust optimization for integrated planning of electric-bus charger deployment and charging scheduling. Transp. Res. Part D: Transp. Environ. 110, 103410.